9-24-2015 12:00 AM

Transmission of light in nano-hole metamaterial

Shankaranandh Balakrishnan .
The University of Western Ontario

Supervisor
Dr. Mahi R. Singh
The University of Western Ontario Joint Supervisor
Dr. Jeffrey Carson
The University of Western Ontario

Graduate Program in Physics
A thesis submitted in partial fulfillment of the requirements for the degree in Master of Science

Transmission of light in nano-hole metamaterial

(Thesis format: Integrated Article)

by

Shankaranandh Balakrishnan

Graduate Program in Physics

A thesis submitted in partial fulfillment
of the requirements for the degree of
Masters of science

The School of Graduate and Postdoctoral Studies
The University of Western Ontario
London, Ontario, Canada

Abstract

The interaction of light with metallic nano-hole array structures enable excitation of surface plasmon polaritons at any angle of incidence. Nano-hole array structure can transmit more radiation than incident light due to the presence of surface plasmon polaritons. This phenomenon has opened up possibilities for a wide range of applications such as Surface Plasmon Resonance sensing and Surface Enhanced Raman spectroscopy.

In this thesis, quantum scattering theory and quantum density matrix method are employed to assess optical transmission of metallic nano-hole array structures. The scattering cross section spectrum is calculated for nano-hole array structures with different nano-hole radii and periodicities and the transmission coefficient is calculated for different angles of incidence. It is found that each measured spectrum has several peaks due to surface plasmon polaritons and the surface plasmon polaritons spectral peaks are dependent on the array periodicity, radius of the nano-holes and the angle of incidence of light. The theoretical predictions are compared with the experimental results and it is found that there is a good agreement between experiments and theory.

The transmission and reflection coefficient of coupler made up of nano-hole array structure is studied and it is found that by modifying the periodicity of the nano-holes, the reflection and transmission properties of the coupler is changed.

Keywords

Nano-hole array, surface plasmon polaritons, optical transmission, scattering cross section, transmission coefficient, density matrix method, coupler.

To my parents

Balakrishnan and Narayani

Acknowledgments

Firstly, I would like to express my sincere gratitude to my advisors Prof. Mahi R. Singh and Dr. Jeffrey Carson for their continuous support of my master's study and related research, for their patience, guidance, motivation and immense knowledge. Their guidance helped me in all the time of research and writing of this thesis. I could not have imagined having a better advisors and mentors for my masters.

Besides my advisors, I would like to thank my thesis committee: Dr. Eugene Wong and Dr. Tammie Poepping for their insightful comments and encouragement, but also the hard question which incented me to widen my research from various perspectives. My sincere acknowledgement goes to every faculty and staff member in the department of Physics and Astronomy at Western university.

My sincere thanks also goes to Dr. Mohamadreza Najiminaini for his valuable inputs in the research project, provision of experimental results and encouragement, and Dr. Astrid Chamson-Reid for her encouragement and support. I would like to thank my fellow lab-mates and friends Marek Brzozowski and Kieffer Davieau for the discussions on research, for all the support and fun we have had in last two years. Also I thank my friends Sharath, Sridhar, Nilesh, Archana, Aishwarya, Rajesh and Divya for their constant motivation and support. I may have never got through the experience without their camaraderie and inspiration.

Last but not the least, I would like to thank my family for their immeasurable love and support throughout my life. Thank you for your prayers everyone, and with God's grace I can do my best.

Table of Contents

List of Abbreviations

EM	Electro-Magnetic
NHA	Nano-Hole Array
EOT	Extraordinary Optical Transmission
FDTD	Finite Difference Time Domain
FET	Finite Element Method
NSOM	Near-field scanning optical microscopy
PIC	Photonic integrated circuit
SERS	Surface Enhanced Raman Spectroscopy
SNOM	Scanning near-field optical microscopy
SOI	Silicon-on-insulator
SP	Surface Plasmon
SPP	Surface Plasmon Polaritons
SPR	Surface Plasmon Resonance
TL	Transmission Line
TM	Transverse Magnetic

List of Figures

Chapter 1

Introduction

1.1 Overview

In the twentieth century, there was a considerable interest towards subwavelength holes as the technology shifted towards longer wavelengths of the electromagnetic spectrum which led to the emergence of microwave technology during the second world war microwave technology was used. A subwavelength hole in an opaque thin metallic film has applications in scanning near-field optical microscopy (SNOM) [1]. Bethe theoretically calculated the transmission of light through the subwavelength hole in a perfectly conducting infinitely thin metal film [2]. According to him, transmission of light through the subwavelength hole is very small. However, experimental results revealed that there was an enhanced transmission at the longer wavelenth for subwavelength holes fabricated in Ag film contradicting Bethe's theory [3]. This is due to the fact that Bethe's theory was for an idealized case which did not consider the surface waves which exist at the metal/dielectric interface. The surface wave plays a significant role in the transmission of light through the subwavelength hole.

In 1998, Thomas W. Ebbesen discovered that there was an extraordinary transmission of light through a nano-hole array structure [4]. Ever since then, there has been considerable efforts devoted to the study of optical properties of metallic nano-hole array (NHA) structures experimentally and theoretically [4]-[9]. These structures allow incident light to couple with surface plasmon present at the metal-dielectric on one side of the metal and decouple on the other side of the film [10], [11]. This mechanism results in extraordinary optical transmission (EOT) of light. The optical transmission properties of NHA depend greatly on the geometrical parameters such as hole shape, hole size and periodicity and material composition (i.e. metal and surrounding dielectric) [12]-[16]. For example, the transmission efficiency of an NHA structure made from noble metals outperforms other structure made from regular metals. S. G. Rodrigo et. al. found that NHA fabricated on noble metals such as gold has higher optical transmission than other metals such as Ag, Cu [17]. This makes gold a natural choice to fabricate NHA structure for sensing applications. A. Krishnan et. al. demonstrated the strong response of metallic NHA structure to changes in refractive index of top and bottom of the metal. They found that by matching the refractive index of top and bottom of the metal, the high transmission can be further enhanced [16].

The intimate connection between optical transmission and the composition and geometry of the NHA have been exploited for wide range of applications such as surface plasmon resonance (SPR) sensing, surface enhanced Raman scattering (SERS), near-field scanning optical microscopy (NSOM), optical filters, optical trapping, absorption spectroscopy, non-linear optics [18]-[22]. Recently it has been found that couplers can be fabricated from

NHA structure in photonic integrated circuits (PICs) for optical communications. Grating couplers are of greater interest in integrated photonics for coupling of light between the waveguides. The coupling is achieved by forming grating couplers in the waveguides. Many works have studied the coupling of light between waveguide and single mode fibre using 1-D grating couplers [23]-[26]. It has been found that these grating couplers achieve high coupling efficiency [27]-[28]. Chen et. al , for the first time, studied coupling between silicon-on-insulator (SOI) waveguide and optical fiber using nano-hole grating coupler [29]. They found that a coupling efficiency as high as 34% was achieved.

However, optimization of NHA structures for sensing and imaging applications has generally been performed with simulation. Finite difference time domain (FDTD) and finite element method (FEM) have been employed to simulate the interaction of light with NHA structures [30]-[34]. The current simulation methods are powerful and accurate but their use for optimization of NHA designs can be a cumbersome process [35]. The coupled-wave analysis method to solve Maxwell's equations in the NHA structures has also been employed [36]-[37]. Chandezon numerical method is one of the most widely used methods to estimate EOT in NHA structures [38]-[39]. It is based on the transformation of the Maxwell equations from the Cartesian coordinates to curvilinear coordinates [38]. Furthermore, simulations often do not provide clear physical insight into the parameters most important for improving device performance.

Theoretical analysis doesn't suffer from the limitations of simulation. Theory provides the advantage of direct interpretation of the optical characteristics' dependence on the material and geometrical parameters. Furthermore, theory provides a means to optimize

the NHA for desirable optical characteristics. Current theoretical descriptions of NHA structures have been developed using transfer matrix formalism and classical physics [40]-[48]. Martin-Moreno and Gracia-Vidal [49] studied the transmission between two localized states by treating it as one dimensional quantum mechanical system.

To overcome some of the limitations of the currently used theoretical descriptions of NHA structures, we present theoretical descriptions of the transmission of light through metallic NHA structures, where the NHA structure is considered as a plasmonic metamaterial [50], [51]. We have also studied the transmission and reflection coeffcient in couplers fabricated from nano-hole array structure.

1.2 Outline of the thesis

The aim of the thesis is to study the transmission of light in metallic NHA structure using quantum theory. The NHA structure is fabricated in optically thick gold film on a pyrex substrate. The NHA system is capable of carrying SPPs propagating at the metal-pyrex interface. The motivation behind this work is that the theoretical analysis of transmission through NHA structure on a pyrex substrate based on quantum theory gives a better insight to optimize the NHA for desirable optical characteristics.

In chapter 2, we will explain the fundamental concepts needed to understand the thesis. The physical concepts such as plasmons, surface plasmon polaritons, metamaterials, scattering cross section, transmission coefficient, density matrix method and experimental procedures are explained.

In chapter 3, the light-matter interaction in metallic nano-hole array structures

is investigated. The scattering cross section spectrum is calculated for three samples each having a unique nano-hole array radius and periodicity for normal incident of light. It is found that each scattering cross section spectrum has several peaks due to surface plasmon polaritons. The dispersion relation for SPPs is calculated using transmission line theory and Bloch's theorem and it is found that the energies of surface plasmon polaritons are quantized. The polarizability of the NHA is also calculated to find the SPP resonance energies and is verified with that found from the dispersion relation. The position of the peaks can be controlled by modifying the periodicity of the nano-hole array structure. The SPP energies obtained from the dispersion relation and polarizability is used to calculate the scattering cross section of the nano-hole array structure. Good agreement was observed between the experimental and theoretical results. It is proposed that the newly developed theory can be used to facilitate optimization of nanosensors for medical and engineering applications.

In chapter 4, the angle dependence transmission coefficient of the metallic nano-hole array structure is calculated. The expression for angle dependence SPPs is derived using the transfer matrix method and Bloch theorem to explain the experiments. The transmission coefficient is calculated using the quantum density matrix method. In this method, one uses the average of an operator on wave functions as well as the statistical ensemble of the system. In this theory, the correlation and coherence effects between SPP modes are included automatically. It is found that there is a fairly good agreement between experimental transmission coefficient and that using the quantum density matrix method. The calculations predict that as the incident angle increases, the number of peaks increases.

It is also found that the position of transmission peaks red/blue shifts depending on the modes. It is also found that the location of the surface plasmon polariton and heights of the spectral peaks are dependent on the angle of incidence of light. Good agreement is observed between the experimental and theoretical results. This property of these structures has opened up new possibilities for sensing applications.

In chapter 5, the optical sensing mechanism of photonic coupler fabricated from the metallic nano-hole array structure, also known as nano-hole array (NHA) coupler, is studied. The metallic nano-hole array structure is embedded between two dielectric material waveguides, with this structure called a metallic nano-hole array coupler. Using the transfer matrix method and coupled-mode theory, expressions for the reflection and transmission coefficients of electromagnetic wave propagating in waveguides have been obtained. It is found that for certain energies, the electromagnetic wave is totally reflected from the coupler. Similarly, for a certain energy range the light is totally transmitted. It has also been found that by changing the periodicity of the metallic nano-hole array, the transmitted energy can be reflected. The periodicity of the metallic nano-hole array can be modified by applying an external stress or pressure. In other words, the system can be used as stress and pressure sensors. The present findings can be used to make new types photonic sensors.

In chapter 6 , the important results of the thesis are summarized and possible future work is discussed.

Bibliography

[1] C. Genet and T. W. Ebbesen, Nature 445(4), 39 (2007).

[2] H. A. Bethe, Phys. Rev., 66, 163(1944)

[3] A. Degiron, H. J. Lezec, N. Yamamoto and T. W. Ebbesen, Opt. Commun 239(1), 61 (2004).

[4] T. W. Ebbesen, H. J. Lezec, H. F. Ghaemi, T. Thio and P. A. Wolf, Nature 391, 667 (1998).

[5] Y. Pang, and R. Gordon, Nano Lett. 12(1), 402-406 (2012).

[6] F. Przybilla, A. Degiron, J-Y Laluet, C. Genet and T. W. Ebbesen, J. Opt. A-Pure Appl. Op. 8(5), 458 (2006).

[7] M. Najiminaini, F. Vasefi, B. Kaminska, and J. J. L. Carson, Appl. Phys. Lett. 100(6), 063110 (2012).

[8] M. Najiminaini, F. Vasefi, B. Kaminska, and J. J. L. Carson, Appl. Phys. Lett. 100(4), 043105 (2012).

[9] R. Gordon, A. G. Brolo, D. Sinton and K. L. Kavanagh, Laser & Photon. Rev., 1 (2009).

[10] H. F. Ghaemi, T. Thio, D. E. Grupp, T. W.W Ebbesen and H. J. Lezec, Phys. Rev. B 58(11), 6779 (1998).

[11] L. Martin- Moreno, F. J. Garcia-Vidal, H. J. Lezec, K. M. Pellerin, T. Thio, J. B. Pendry and T. W. Ebbesen, Phys. Rev. Lett., 86(6), 1114 (2001).

[12] Y. Pang and R. Gordon, Nano Lett. 12(1), 402 (2012).

[13] F. Przybilla, A. Degiron, J. Y. Laluet, C. Genet and T. W. Ebbesen, I. Opt. A, Pure Appl. Opt. 8(5), 458 (2006).

[14] M. Najiminaini (2012), Development of 3D metallic nano-structures for sensing applications, Ph.D thesis. Simon Fraser University.

[15] R. Gordon, A. G. Brolo, A. McKinnon, A. Rajora, B. Leathem and K. L. Kavanagh, Phys. Rev. Lett 92(3), 037401 (2004).

[16] A. Krishnan, T. Thio, T. J. Kim, H. J. Lezec, T. W. Ebbesen, P. A. Wolff, J. Pendry, L. Martin-Moreno, F. J. Garcia-Vidal, Opt. Commun 200, 1 (2001).

[17] S. G. Rodrigo, F. J. Garcia-Vidal, and L. Martin-Moreno, Phys. Rev. Lett. B 77, 075401 (2008).

[18] R. Gordon, A. G. Brolo, D. Sinton and K. L. Kavanagh, Laser Photon. Rev. 4(2), 311 (2010).

[19] A. G. Brolo, S. C. Kwok, M. G. Moffitt, R. Gordon, J. Riordon and K. L. Kavanagh, J. Am. Chem. Soc. 127(42), 14936 (2005).

[20] J. R. Lakowicz, M. H. Chowdhury, K. Ray, J. Zhang, Y. Fu, R. Badugu, C. R. Sabanayagam, K. Nowaczyk, H. Szmacinski, K. Aslan and C. D. Geddes, Proc SPIE 6099, 9-1 (2009).

[21] A. Lesuffleur, H. Im, N. C. Lindquist, K. S. Lim and S. H. Oh, Opt. Express 16(1), 219 (2008).

[22] F. M. Huang, Y. Chen, F. J. Garcia de Abajo and N. I. Zheludev, Appl. Phys. Lett. 90(9), 091119 (2007).

[23] D. Taillert, W. Boagerts, P. Bienstman,T. F. Krauss, P. Van Daele, I. Moerman, S. Verstuyft, K. De Mesel and R. Baets, IEEE, J. Quant. Electron. 38 (7), 949 (2002).

[24] F. Van Laere, G. Roelkens, M. Ayre, J. Schrauwen, D. Tillaert, D. Van Thourhout, T. F. Krauss and R. Baets, J. Lightwav Technol. 25 (1), 151 (2007).

[25] B. Wang, J. Jiang and G. P. Nordin, IEEE Photon. Technol. Lett 17 (9), 1884 (2005).

[26] V. Dolores-Calzadilla, D. Heiss and M. Smit, Opt. Lett. 39 (9), 2786 (2014).

[27] N. Eriksson, M. Hagberg and A. Larsson, IEEE J. Quantum Electron., 32, 942 (2000).

[28] T. W. Ang, G. T. Reed, A. Vonsovici, A. G. R. Evans, P. R. Routley and M. R. Josey, IEEE Photon. Technol. Lett., 12, 59 (2000).

[29] X. Chen and H. K. Tsang, IEEE Photon. J. 1 (3), 184 (2009).

[30] Y. Wang,Y. Qin, and Z. Zhang, Plasmonics 9(2), 203(2014).

[31] S-H Chang, and S. K. Gray, Opt. Express. 13(8), 3150(2005).

[32] I. Ashry, A. Elrashidi, M. M. Tharwat, Y. Xu, and A. M. Mahros, Plasmonics 10(3), 511 (2014).

[33] J. M. McMahon, J. Henzie, T. W. Odom, G. C. Schatz, and S. K. Gray, Opt. Express 15 (26), 18119 (2007).

[34] X. Pang, C. Y. Zhao, and H. Bao, J. Quant. Spectrosc. Radiat. Transfer 133, 579 (2014).

[35] M. Najiminaini, F. Vasefi, B. Kaminska, and J. J. L. Carson, Opt. Express 18 (21), 22255 (2010).

[36] M. Nishida, N. Hatakenaka, and Y. Kadoya, Multipole surface plasmons in metallic nanohole arrays, arXiv:1502.05549v2 (2015).

[37] G. X. Li, Z. L. Wang, S. M. Chen, and K. W. Cheah, Opt. Express 19 (7), 6348 (2011).

[38] J. Chandezon, M. T. Dupuis, G. Cornet, and D. Maystre, J. Opt. Soc. Am. 72, 839–846 (1982).

[39] L. Li, J. Opt. Soc. Am. A 11, 2816–2828 (1994).

[40] P. Lalanne, C. Sauvan, J. P. Hugonin, J. C. Rodier and P. Chavel, Phys. Rev. B 68, 125404 (2003).

[41] M. Zhang, C. Huang, G. Wang and Y. Zhu, J. Opt. 12, 015004 (2010).

[42] J.A. Porto, F.J. Garcia-Vidal, and J. B. Pendry, arXiv:cond-mat/9904365v1[cond-mat.mtrl-sci] (1999).

[43] N. Garcia, and M. Bai, Optical Express 14, 10028(2006).

[44] X. Fang, C. Y. Zhao, and H. Bao, Journal of Quantitative Spectroscopy and Radiative Transfer 133(0), 579 (2014).

[45] U. Schroter, and D. Heitmann, Phys. Rev. B 58(23), 15419 (1998).

[46] E. Popov, M. Nevière, S. Enoch, and R. Reinisch, Phys. Rev. B 62(23), 16100 (2000).

[47] H. Shin, P. B. Catrysse, and S. Fan, Phys. Rev. B 72 (8), 085436 (2005).

[48] J. Porto, F. Garcia-Vidal, and J. Pendry, Phys. Rev. Lett. 83(14), 2845 (1999).

[49] L. Martin-Moreno and F. Garcia-Vidal, Opt. Express 12(16), 3619 (2004).

[50] F. J. Garcia-Vidal , L. Martin-Moreno, J. B. Pendry, J. Opt. A 7, S97 (2005).

[51] C. Carloz and T. Itoh, Electromagnetic Metamaterials, Wiley Interscience, Hoboken, New Jersey (2006).

Chapter 2

Fundamentals

In this chapter, the fundamental concepts required in the thesis are discussed. In this thesis, we have used terms such as plasmons, surface plasmon polaritons, scattering cross section, density matrix method, etc.

2.1 Plasmons in metal

In this section, we calculate the dispersion relation for metals. The following material is taken from reference [1], [2].

It's a well-known fact that the metals contain free elctrons called conduction electrons. These conduction electrons oscillate in the presence of an external electromagnetic field. Let us consider a metal which contains the number of electrons per unit volume, n_e. The mass and charge of an electron is denoted as m_e and e respectively. Let us apply an electromagnetic (EM) field

$$\mathbf{E} = \mathbf{E}_0 e^{-i\omega t} \tag{2.1}$$

where $\mathbf{E}_0$ is the amplitude and ω is the frequency of the EM field. The EM field induces oscillatory dipole moments defined by $\mathbf{p}_e$ in the metal due to the electron oscillation within the conduction band. Therefore, the equation of motion of the free electrons in the presence of EM field is written as

$$m_e \frac{d^2\mathbf{r}}{dt^2} = \gamma_m m_e \frac{d\mathbf{r}}{dt} - e\mathbf{E}_0 e^{-i\omega t} \tag{2.2}$$

The first term on the right hand side is called the damping force due to the collisions of the electron with phonons and impurities and the second term is the electric force. Here γ_m is called the damping constant.

The electron oscillates with the same frequency as the electric field. Therefore, the solution to the above equation can be written as

$$\mathbf{r} = \mathbf{r}_0 e^{-i\omega t} \tag{2.3}$$

where $\mathbf{r}_0$ is the amplitude of oscillation. Putting eqn. (2.3) into eqn. (2.2), it reduces to

$$\mathbf{r}_0 = \frac{\frac{e}{m_e}\mathbf{E}_0}{\omega^2 + i\gamma_m\omega} \tag{2.4}$$

The polarization $\mathbf{P}$ of the metal is defined as the dipole moment $\mathbf{p}_e$ per unit volume and is expressed as

$$\mathbf{P} = n_e \mathbf{p}_e \tag{2.5}$$

Putting $\mathbf{p}_e = -e\mathbf{r}$ and eqn. (2.3) into eqn. (2.5), we get

$$\mathbf{P} = \alpha_e \mathbf{E}_0 e^{-i\omega t} \tag{2.6}$$

where α_e is called as the polarizability and it is defined as

$$\alpha_e = -\frac{\frac{e^2}{m_e}}{\omega^2 + i\gamma_m\omega} \tag{2.7}$$

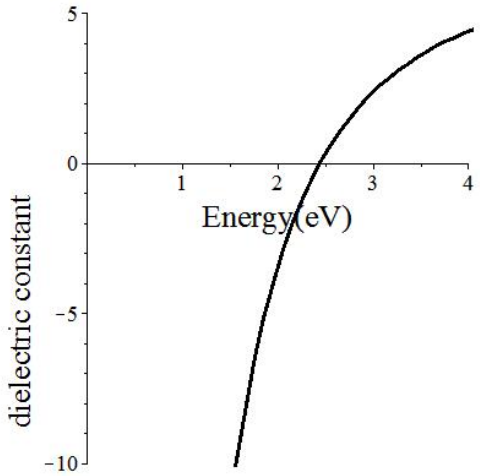

Figure 2.1: Dielectric constant as a function of energy (eV). Note that for $\omega < \omega_p$, ϵ_m is negative.

The dielectric function of metals ϵ_m is defined as the ratio of the displacement vector $\mathbf{D}$ to the applied electric field $\mathbf{E}$ where the displacement vector is defined as $\mathbf{D} = \mathbf{E} + \mathbf{P}/\epsilon_0$

$$\epsilon_m = \frac{\mathbf{E} + \mathbf{P}/\epsilon_0}{\mathbf{E}} \tag{2.8}$$

Putting eqn. (2.1) and eqn. (2.6) into eqn. (2.8), we get the expression for the dielectric constant as

$$\epsilon_m = 1 - \frac{\omega_p^2}{\omega^2 + i\gamma_m\omega} \tag{2.9}$$

where the quantity ω_p is called the plasma frequency and is defined as

$$\omega_p = \sqrt{\frac{n_e e^2}{m_e \epsilon_0}} \tag{2.10}$$

Thus, the electrons in metals oscillate collectively with the plasmon frequency ω_p. The dielectric constant of the metal is plotted in Fig. 2.1. The frequency at which the dielectric constant becomes zero is called the plasmon energy ω_p. Note that for $\omega < \omega_p$, ϵ_m is negative, which is an interesting property of metals. This effect is very important to study

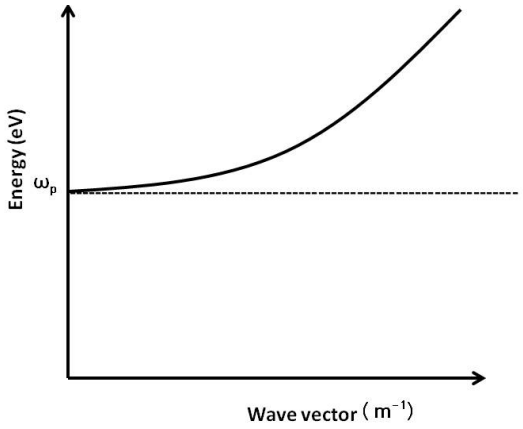

Figure 2.2: Dispersion relation for plasmons in metals. Note that the wave doesn't propagate for frequencies between $\omega = 0$ and $\omega = \omega_p$.

the surface plasmon polaritons in metallic heterostructures.

The dispersion relation for photons in metals is given by

$$k = \frac{\omega}{c}\sqrt{\epsilon_m} \tag{2.11}$$

Eqn. (2.11) is called the dispersion relation between k and ω. The dispersion relation for photons in metal is plotted in Fig 2.2.

Putting eqn. (2.9) in eqn. (2.11), the dispersion relation becomes

$$k = \frac{\omega}{c}\sqrt{1 - \frac{\omega_p^2}{\omega^2 + i\gamma_m\omega}} \tag{2.12}$$

Note that for $\omega > \omega_p,\ k$ is positive (i.e. $k = +|k|$) . This gives

$$\mathbf{E}(r,t) = \mathbf{E}(r)e^{i|k|r}e^{i\omega t} \tag{2.13}$$

For $\omega < \omega_p,\ k$ is an imaginary quantity (i.e. $k = +i|k|$). This gives

$$\mathbf{E}(r,t) = \mathbf{E}(r)e^{-|k|r}e^{i\omega t} \tag{2.14}$$

This means for $\omega > \omega_p$, EM wave propagates inside the metal. However for $\omega < \omega_p$, the EM decays in the metal and doesn't propagate in the metal but is reflected. The dispersion relation for the metal is plotted in Fig. 2.2. Note that the EM wave doesn't propagate between $\omega = 0$ and $\omega = \omega_p$.

2.2 Surface Plasmon Polaritons in metallic heterostructures

When an electromagnetic field is applied to a metallic heterostructure, it couples to plasmons at the surface. In other words, the EM wave and surface plasmons interact at the surface of the metals. The coupled EM wave-surface plasmons system creates new particles called surface plasmon polaritons (SPPs).

Let us calculate the dispersion relations for SPPs in the metallic heterostructure as given in reference [1], [3] by solvingMaxwell's equation for metal and dielectric heterostructure for transverse magnetic (TM) modes. A schematic diagram of metallic heterostructure is shown in the Fig. 2.3.The dielectric constant of the dielectric and metallic materials are denoted as ϵ_d and ϵ_m respectively. Let us consider that both the materials lie in $y-z$ plane with their interface lie at $x = 0$. Maxwell's equation is written as

$$\nabla^2 \mathbf{H}_{dy} = \left(\frac{\omega}{c}\right)^2 \varepsilon_d \mathbf{H}_{dy} \qquad x > 0 \tag{2.15}$$

$$\nabla^2 \mathbf{H}_{my} = \left(\frac{\omega}{c}\right)^2 \varepsilon_m \mathbf{H}_{my} \qquad x < 0 \tag{2.16}$$

The solution to the Maxwell's equation is written as

$$H_{dy}(x) = B_d e^{-k_{dx}x} e^{ik_z z} \qquad x > 0 \tag{2.17}$$

$$H_{my}(x) = B_m e^{k_{mx}x} e^{ik_z z} \qquad x < 0 \tag{2.18}$$

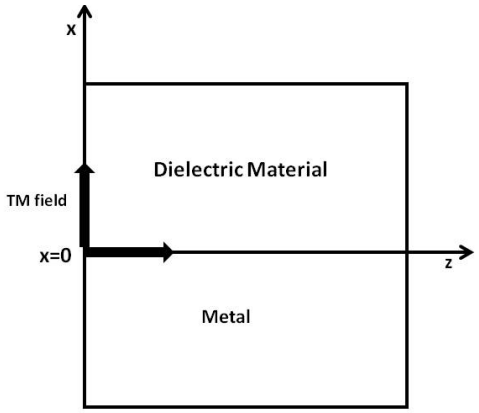

Figure 2.3: A schematic diagram of a heterostructure made from a metal and a dielectric material.

where B_d and B_m are the amplied of the EM field inside the dielectric and metal respectively. Here k_{dx} and k_{mx} are the wave vectors along the positive x direction in dielectric material and negative x direction in metal and are defined as

$$k_{dx} = \sqrt{\frac{\epsilon_d \omega^2}{c^2} - k_z^2} \tag{2.19}$$

$$k_{mx} = \sqrt{\frac{\epsilon_m \omega^2}{c^2} - k_z^2} \tag{2.20}$$

where k_z is the propagating wave vector. Note that when k_z is positive EM waves propagate along z direction and decays along the x direction when k_d and k_m have positive values. We use the boundary condition that $H_{dy}(x)$ and $H_{my}(x)$ must be continous at $x = 0$. i.e.

$$[H_{dy}(x)]_{x=0} = [H_{my}(x)]_{x=0} \tag{2.21}$$

$$\left[\frac{dH_{dy}(x)}{dx}\right]_{x=0} = \left[\frac{dH_{my}(x)}{dx}\right]_{x=0} \tag{2.22}$$

Putting eqns. (2.17) and (2.18) into eqns. (2.21) and (2.22) and using eqns (2.19) and

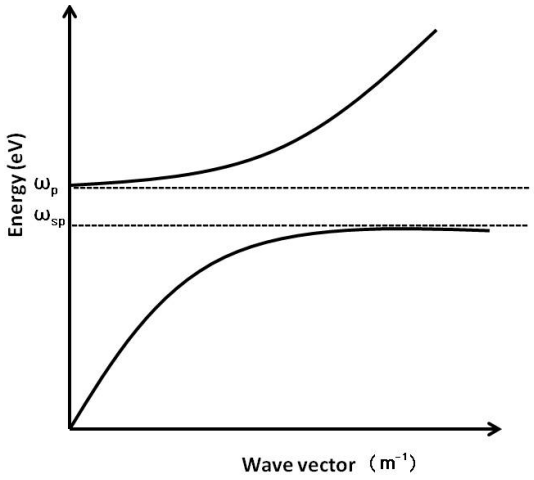

Figure 2.4: Dispersion relation for surface plasmon polaritons in a metallic heterostructure. The curve above the ω_p line (i.e. $\omega > \omega_p$) is the propagated wave whereas the curve below ω_{sp} line (i.e. $\omega < \omega_{sp}$) is the SPP wave.

(2.20), we get

$$k_z = \frac{\omega}{c}\sqrt{\frac{\epsilon_m \epsilon_d}{\epsilon_m + \epsilon_d}} \tag{2.23}$$

The above equation is called the dispersion relation for the surface plasmon polaritons. It is plotted in Fig. 2.4. Note that for $\omega > \omega_p$, the wave vectors k_z is real and k_{mx} and k_{dx} are imaginary. This means that the terms $e^{ik_{dx}x}$ and $e^{-ik_{mx}x}$ EM wave propagates along the x direction. The term $e^{ik_z x}$ term of the EM wave propagates along the z direction. These waves are called radiative polaritons. For $\omega < \omega_{sp}$, the wave vectors k_z is real and k_{mx} and k_{dx} are real. This means that the terms $e^{-k_{dx}x}$ and $e^{k_{mx}x}$ EM wave decays in the x direction. The term $e^{ik_z x}$ term of the EM wave propagates along the z direction. These waves are called localized surface plasmon polaritons (SPPs).

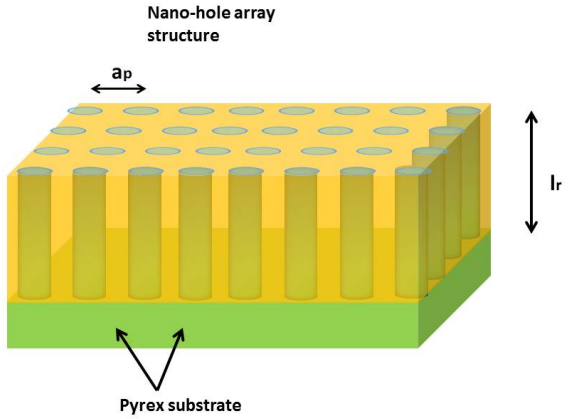

Figure 2.5: A schematic diagram of nano-hole array structure on a Pyrex substrate.

2.3 Nano-hole array (NHA) structure and Metamaterials

Nano-hole array structure is an array of periodic subwavelength hole aperture fabricated in thin metal film. The size and spacing of the holes are smaller than the wavelength of the light. These structures enable excitation of surface plasmons which leads to extraordinary transmission of incident light. A schematic diagram of metallic nano-hole array structure on pyrex substrate is shown in Fig. 2.5. These structure are also called as photonic metamaterials. Photonic metamaterials are periodic optical nanostructures often composed of metallic elements where the period is shorter than the wavelength of the light. They are of large scientific interest as the dielectric response of these materials can be engineered to yield interesting physical phenomena at optical wavelengths.

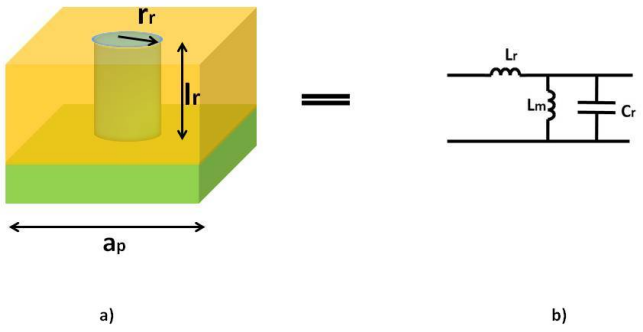

Figure 2.6: a) A schematic representation of the unit cell of nano-hole array structure. b) Equivalent L-C circuit diagram of the unit cell.

2.4 Photons in nano-hole array structure

In this section, we calculate the dispersion relation of nano-hole array structure using the method of reference [4]. The unit cell of NHA is shown in Fig. 2.6a. Note that the unit cell contains one nano-hole rod. An electromagnetic (EM) wave is applied to the NHA structure. The component of the electric field E of the EM wave oscillates with frequency ω, creating an oscillatory current at the surface of nano-hole. This oscillator current produces a magnetic field within the unit cell. Therefore the unit cell acts as inductor and capacitor as shown in Fig. 2.6b.

Let us calculate the dispersion relation of metallic nano-hole array structure. To calculate the dispersion relation, we use the transmission line (TL) theory which is used widely in metamaterial physics [4], [5]. In this theory the unit cell is replaced with an L-C circuit as shown in Fig. 2.6b. Therefore we can calculate the impedance (Z_s) and an

admittance (Y_s) as shown in the figure as follows [4]

$$Y_s = i\omega C_r + \frac{1}{i\omega L_r} \tag{2.24}$$

$$Z_s = i\omega L_m \tag{2.25}$$

where L_m and C_r are called the inductance and capacitence per unit length of the rod respectively. The inductance L_r of metallic hole rod is calculated in reference [4] and it is written as

$$L_r = \frac{\mu_0 a_p}{2\pi}\left[\ln\left(\frac{2l_r}{r_r}\right) - \frac{3}{4}\right] \tag{2.26}$$

where μ_0 is the permeability in free space. Here r_r is radius of the nano-hole, l_r is the length of the rod and a_p is the periodicity of the NHA structure.

The expression for the dispersion relation of the nano-hole array structure is calculated in ref [4] as

$$\cos(k_s a_p) = 1 + \frac{Y_s Z_s}{2} \tag{2.27}$$

where k_s is the wave vector of EM wave in the metallic NHA structure.

Putting the eqns. (2.24) and (2.25) into eqn. (2.27), and using $\cos(k_s a_p) = 1 - 2\sin^2(k_s a_p/2)$, we get the following expression for dispersion relation

$$k_s = \frac{2}{a_p}\arcsin\left(\frac{\omega}{\sqrt{2}\omega_m}\sqrt{1 - \frac{\omega_p^2}{\omega^2 + i\gamma_m\omega}}\right) \tag{2.28}$$

where γ_m is the decay rate due to the energy loss in the nano-hole structure. The parameters ω_p and ω_m are defined as

$$\begin{aligned} \omega_p &= \sqrt{\frac{1}{C_r L_r}} \\ \omega_m &= \sqrt{\frac{1}{C_r L_m}} \end{aligned} \tag{2.29}$$

The dielectric constant of the metallic NHA structure can be calculated from the dispersion relation and it is given as

$$\varepsilon_s = \left[\frac{2c}{a_p \omega} \arcsin \left(\frac{\omega}{\sqrt{2}\omega_m} \sqrt{1 - \frac{\omega_p^2}{\omega^2 + i\gamma_m \omega}} \right) \right]^2 \tag{2.30}$$

Using eqn (2.30), the dispersion relation for the SPPs in NHA structure on a pyrex substrate is calculated in chapter 3. It is found the energy ε_n of SPPs is quantized where $n = 0, 1, 2$.

2.5 Transmission coefficient of light in nano-hole array structure

As we discussed in the previous section that the surface plasmon polaritons (SPPs) in the nano-hole array structure on pyrex susbtrate have quantized energy ε_n with eigen ket $|n\rangle$. Let us consider that there are two SPP states in the NHA structure. Therefore, the SPP modes participating in the transmission process have energies ε_0 and ε_1.The ground state is denoted by $|0\rangle$ with energy ε_0. The next excited state is denoted by $|1\rangle$ with state ε_1 (see the schematic diagram Fig 2.7).

The transmission coefficient T_{trans} of the nano-hole array structure due to absorption and emission of SPPs between the between the states $|0\rangle$ and $|1\rangle$ is expressed as [3]

$$T_{trans} = \alpha_0 \, \mathrm{Im}(\rho_{01}) \tag{2.31}$$

where

$$\alpha_0 = \frac{\mu_{01} \varepsilon_p}{\hbar E_p c} \tag{2.32}$$

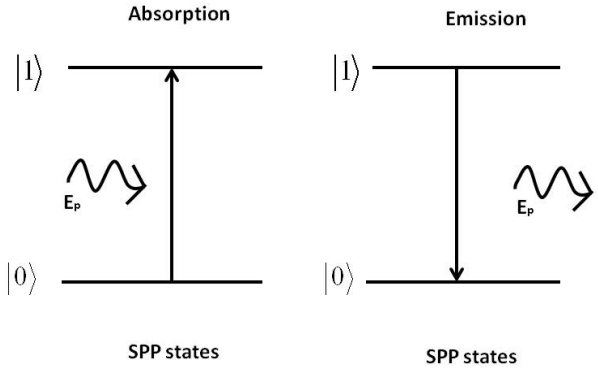

Figure 2.7: Energy level diagram of transmission process. The SPP will absorb photon of energy $\hbar\omega$ to be taken from ground state to excited state. Once the SPP decays back to the ground state, it emits the photon back.

Here μ_{01} and $\rho_{01}$are dipole and density matrix elements between states $|0\rangle$ and $|1\rangle$ respectively. E_p is the amplitude of incident EM field and ε_p is the energy of the incident EM field. The density matrix element ρ_{01} is evaluated using density matrix method. In this method, the density matrix elements are evaluated from the following equation of motion

$$\frac{d\rho(t)}{dt} = -\frac{i}{\hbar}\left[H, \rho(t)\right] \tag{2.33}$$

where H is the total Hamiltonian of the system given by

$$H = H_0 + H_F \tag{2.34}$$

Here H_0 is the non-interacting Hamiltonian of SPP modes and it is written in the second quantized form as [3]

$$H_0 = \varepsilon_0\sigma_{00} + \varepsilon_1\sigma_{11} \tag{2.35}$$

where $\sigma_{nn} = |n\rangle \langle n|$ is called the preservation operator.

H_F is called as the interaction Hamiltonian between EM wave and induced dipole moments and it is written in rotating wave approximation as

$$H_F = -\left[\hbar\Omega_{01}\sigma_{01}^{+}e^{-i\frac{(\varepsilon_{10}-\varepsilon_p)t}{\hbar}}\right] + h.c. \tag{2.36}$$

where $\sigma_{01}^{+} = |1\rangle \langle 0|$ is the SPP creation operator and $\varepsilon_{10} = (\varepsilon_1 - \varepsilon_0)$. Here $h.c$ stands for the Hermitian conjugate and Ω_{01} is called as the Rabi frequency associated with the transition $|0\rangle \leftrightarrow |1\rangle$. Putting eqn. (2.35) and eqn. (2.36) into eqn. (2.34), it becomes

$$H = \varepsilon_0\sigma_{00} + \varepsilon_1\sigma_{11} - \left[\hbar\Omega_{01}\sigma_{01}^{+}e^{-i\frac{(\varepsilon_{10}-\varepsilon_p)t}{\hbar}}\right] + h.c. \tag{2.37}$$

Solving eqn. (2.33) using the above eqn. (2.37), we obtain the following equations of motion for the density matrix elements (the detailed derivation is given in Appendix B)

$$\begin{aligned} \frac{d\rho_{11}}{dt} &= -2\Gamma_1\rho_{11} - i\left(\Omega_{01}\right)\rho_{01} - i\left(\Omega_{01}\right)^{*}\rho_{10} \\ \frac{d\rho_{10}}{dt} &= -(\frac{\Gamma_1}{2} + i\Delta_{01})\rho_{10} - i\left(\Omega_{01}\right)\left(\rho_{11} - \rho_{00}\right) \end{aligned} \tag{2.38}$$

where $\Delta_{01} = \omega_0 - \omega_1 - \omega$ and $\Delta_{02} = \omega_0 - \omega_2 - \omega$ are called the probe field detunings. Physical quantities $\Gamma_1$and Γ_2 appearing in eqn. (2.38) are the spontaneous decay rates of the levels $|1\rangle$ and $|2\rangle$ respectively. Using the above method, one can evaluate density matrix elements for many SPP states. Solving eqn. (2.38) self-consistently, one can evaluate ρ_{10}. This value can be susbtituted in eqn. (2.31) to calculate the transmission coefficient

2.6 Scattering Cross Section in the nano-hole structure

In the previous section, we have discussed the density matrix method to calculate the the transmission coefficient. In this section, we calculate the transmission coefficient

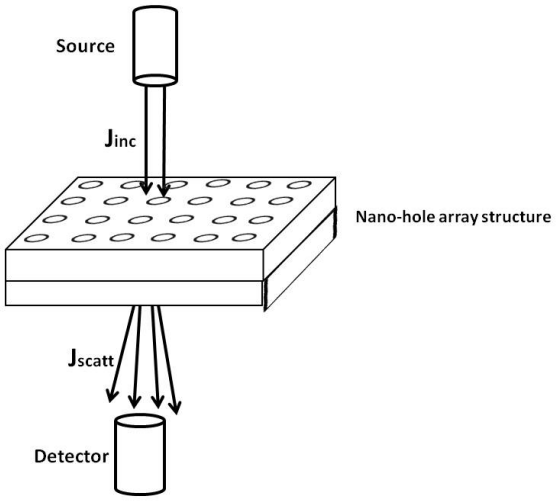

Figure 2.8: A schematic diagram of the scattering process where source is Halogen light. J_{inc} is the incident flux of EM waves and J_{scatt} is the flux of scattered EM waves

using scattering cross section method.

Scattering is a very important process in science. A schematic diagram of the scattering process is shown in Fig. 2.8. The source is a halogen lamp which emits EM wave (photons). The incident light J_{inc} from a light source scatters with the NHA structure. The scattrered light with intensity J_{scatt} is measured by the detector. Therefore, the scattering cross section T_{trans} is defined as [7]

$$T_{trans} = \frac{J_{scatt}}{J_{inc}} \tag{2.39}$$

where J_{inc} and J_{scatt} are defined as

$$J_{scatt} = w_{if}\rho(\varepsilon_{k_n})d\Omega \tag{2.40}$$

$$J_{inc} = \frac{1}{2}\varepsilon_0 E_0^2 \tag{2.41}$$

where $\rho(\varepsilon_{k_n})$ is the density of states of scattered photons and $\rho(\varepsilon_{k_n})d\Omega$ is the number

of photons scattered into the detector, ε_0 is the permitivity of free space and E_0 is the amplitude of the incident field.

The transition probability w_{in} of the system going from initial state i to final state n is given by

$$w_{in} = \left(\frac{2\pi}{\hbar}\right) |V_{int}|^2 \frac{\Gamma_n}{(\varepsilon - \varepsilon_n)^2 + \Gamma_n^2} \tag{2.42}$$

where V_{int} is the matrix elements (between initial and final state) of the interaction Hamiltonian between applied field and the system. Γ_n is the linewidth of the final state of the system. The derivations for the expression for w_{in} and T_{trans} is given in the reference [8] and appendix A.

2.7 Experimental Methods

In this section, we describe the fabrication of nano-hole array structures in gold films and optical characterization of the NHA devices [8]. The fabrication and experimental work was performed by Dr. Mohamdreza Najiminaini.

2.7.1 Fabrication of nano-hole array structure

The electron beam lithography (EBL) was employed and a lift-off process to fabricate nano-hole arrays in a metal film. First, a 500 μm thick Pyrex 7740 wafer was cleaned in sulfuric acid for 5 minutes followed by electron beam deposition of a 3-nm thick Ti layer onto the Pyrex substrate. The Ti layer made the Pyrex surface conductive and allowed EBL on the photoresist layer. Then, a 500-nm thick layer of negative tone photoresist (ma_N

2403, Micro resist technology, Berlin, Germany) was spin-coated onto the Pyrex surface and baked at 90° for 60s. The nano-hole array patterns were written on to the photoresist with the EBL machine (LEO, 1530 e-beam lithography, UWO Nanofab) and the photoresist was subsequently developed (MF-319, Shipley, Marlborough, MA). The process left behind an array of photoresist nano-pillars, which were used as a mask layer during the lift-off. A 3-nm thick Ti layer and a 100-nm thick Au layer were deposited in sequence on to the photoresist nano-pillars (electron beam deposition). The 3-nm thick Ti layer served as an adhesion layer between the substrate and the gold film. Afterwards, the sample was left in 80 PG Remover (MicroChem Corp., Westborough, MA) and sonicated to facilitate the lift-off process. After lift-off, the sample was left in Ti TFTN etchant to remove the Ti conductive and adhesion layers. The end result was a nano-hole array structure in a gold film on top of the Pyrex substrate.The nano-hole arrays in a 100-nm thick gold film on Pyrex substrate with various hole sizes and periodicities was first fabricated where nano holes were distributed in a square lattice. A schematic diagram of a nano-hole array structure on pyrex substrate is shown Fig. 2.9a. The holes were circular in cross-section and had 100 nm, 120 nm, and 140 nm hole diameters and 360 nm, 400 nm, and 440 nm periodicities. A scanning electron microscopy (SEM) image of a portion of a fabricated nano-hole structure is shown in Fig. 2.9b. The same method was employed to fabricate nano-hole arrays in metal on Pyrex substrate having a of 287 nm hole size and 440 nm periodicity.

2.7.2 Optical characterization setup

Fig. 2.10 displays a diagram of the optical setup used to characterize the nano-hole array structures. An inverted microscope (TE 300, Nikon) attached to a photometer

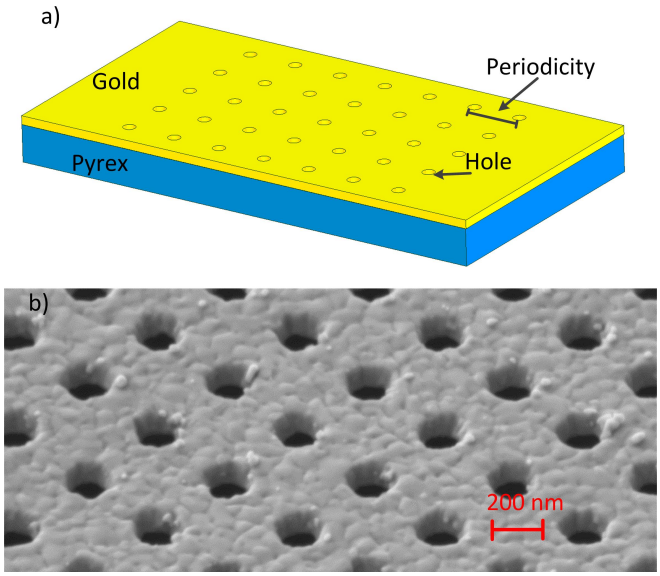

Figure 2.9: a) A schematic diagram of nano-hole array structure in a gold film on a pyrex substrate and b) an SEM image of nano-hole array structure in a gold film on a pyrex substrate

(D104, PTI), monochromator (101, PTI), and photomultiplier tube (710, PTI) was employed to measure optical transmission of each nano-hole array within the spectral range of 400 nm to 870 nm. The microscope utilize a halogen lamp that was focused onto the sample using the bright-field condenser. The aperture of the condenser was set in such a way that the light illumination angle was within 6°. The light transmitted through the sample was collected with a 100X objective lens (plan fluor, NA=0.9, Nikon) and then guided through a photometer. The photometer permitted the selection of a region of interest on the sample using an adjustable horizontal slit and an adjustable vertical slit. Light from the photometer was directed to the monochromator and the output from the monochromator was measured with the photomultiplier tube for each wavelength. To calculate optical transmission through each nano-hole array, the optical system noise (dark noise)

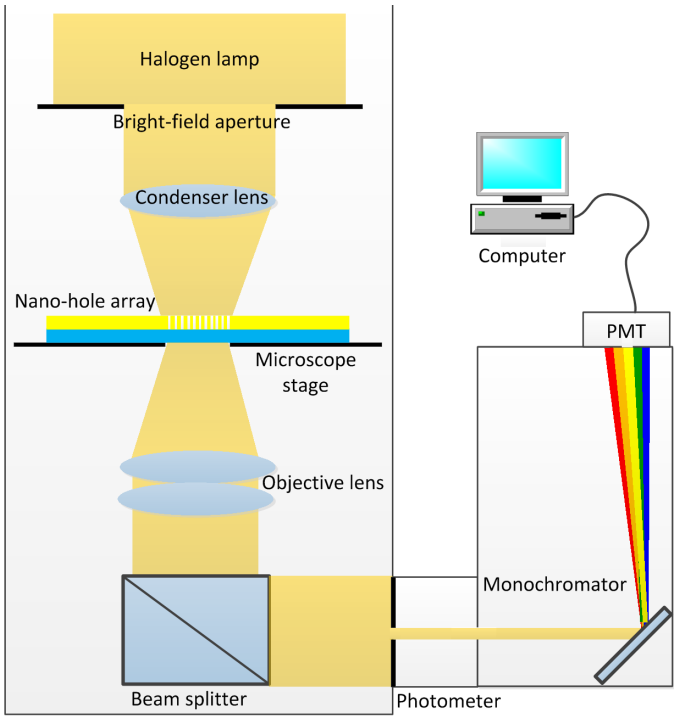

Figure 2.10: Optical characterization setup of nano-hole array structure for normal incidence.

was subtracted from the light intensity transmitted through each nano-hole array and the result was normalized to the light transmission through a bare Pyrex wafer.Optical characterization setup to study the transmission of light for various angles of incidence is shown in the fig. (2.11).An inverted microscope equipped with photometer, monochromator, and photo-multiplier tube was employed for characterizing optical transmission spectra of nano-hole array at various illumination angles. A collimated halogen lamp light was spatially filtered using pin-hole and ring apertures and then focused on the nano-hole array sample to obtain a desired incident angle of light on a nano-hole array. As shown in Figure. 2.11, the utilized pin-hole and ring apertures provide $0^\circ \pm 2^\circ$, $5^\circ \pm 2^\circ$ and $12^\circ \pm 2^\circ$ incident angle of light. The transmitted light through a nano-hole array was collected using 20X

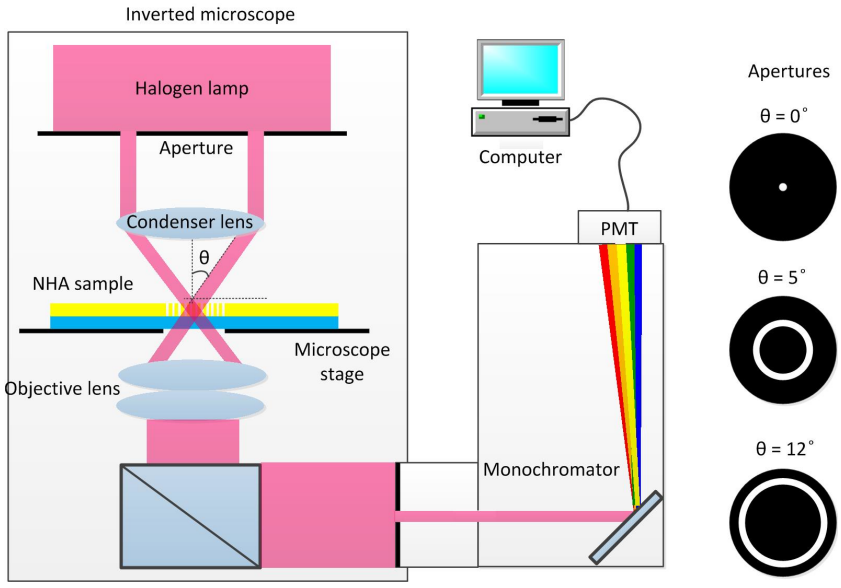

Figure 2.11: Optical characterization setup of nano-hole array structure for different angles of incidence.

objective and guided through photometer using beam-splitter. A region of interest on a nano-hole array sample was selected using photometer and transferred to monochromator for spectral dispersion. The dispersed light was detected and captured by photomultiplier tube and plotted by computer within 500-nm and 850-nm. The optical transmission of a nano-hole array was calculated by subtraction of system dark noise from intensity of light transmitted through a nano-hole array and divided by the transmitted light through bare Pyrex wafer.

Bibliography

[1] M. R. Singh, *Modern Topics in Materials Scienc*e, (John Wiley and Sons, Toronto, 2014).

[2] Lukas Novotny and Bert Hecht, *Principles of Nano-optics*, Cambridge University Press, New York, 2006.

[3] Stefan A. Maier, *Plasmonics: Fundamentals and Applications*, Springerscience + Business media LLC, New York, 2007.

[4] C. Carloz and T. Itoh, *Electromagnetic Metamaterials*, Wiley Interscience, Hoboken, New Jersey, (2006).

[5] R. R. A. Syms, E. Shamonina, V. Kalinin and L. Solymar, J. Appl. Phys. 97, 064909 (2005).

[6] M. R. Singh, *Electronic, Photonic, Polaritonic and Plasmonic Materials* (John Wiley and Sons, Toronto, 2014).

[7] M. R. Singh, *Advanced Quantum Mechanics* (John Wiley and Sons, Toronto, 2014).

[8] M. R. Singh, M. Najiminaini, S. Balakrishnan and J. J. L. Carson, J. Appl. Phys. 117, 184302 (2015).

Chapter 3

Metamaterial-based theoretical description of light scattering by metallic nano-hole array structures[1]

In the previous chapter, the background materials pertaining to the thesis were discussed. In this chapter, we study the dispersion relation for surface plasmon polaritons (SPPs), polarizabiltiy of surface plasmon polaritons (SPPs) and scattering cross section of light in metallic nano-hole array structure.

[1]Reproduced with permission from Mahi R. Singh, Mohamadreza Najiminaini, Shankar Balakrishnan and Jeffrey J. L. Carson, Journal of Applied Physics, vol. 117, 184302 (2015). Copyright 2015, AIP Publishing LLC.

3.1 Introduction

There has been growing interest in developing nanoscale sensing devices using metallic nanomaterial heterostructures [1]-[3]. A very good example of nanomaterial heterostructures is a nano-hole array (NHA) structure fabricated in thin metallic film on pyrex substrate. The interest in developing metallic nano-hole array devices come from their ability to transmit more light than that of incident light [4]. The mechanism is known as extraordinary optical transmission (EOT). The extraordinary optical transmission (EOT) is associated with the interaction of light with surface plasmons (SPs) present at the metal-dielectric interface and the coupling of light with surface plasmons results in new particles called surface plasmon polaritons (SPPs). This unique property has opened up new possibilities for applications such as biosensing.

In this chapter, we present theoretical results of transmission of light through metallic nano-hole array structures at normal incidence. Here the NHA structure is considered as a plasmonic material. A quasi-quantum mechanical theory of scattering cross section based on quantum scattering theory and Green's function method is used to calculate the transmission coefficient. The SPP energies are found to be quantized and the systems can have several SPPs depending on the radius and periodicity of the nano-holes in NHA structures. The optical transmission was calculated as a function of radius and periodicity.There was a good agreement between theory and experiment.

3.2 Surface Plasmon Polaritons in nano-hole array structure

In this section, the dispersion relation for the NHA structure is studied. The nano-holes are arranged periodically in the nano-hole array struture as shown in Fig. 2.5. Each nano-hole is descibed as a cylindrical hollow rod. The radius of the nano-hole is r_r and the length of the nano-hole rod is considered as l_r .The periodicity of the structure is considered as $a_{p.}$ A schematic diagram of the unit cell is shown in Fig. 2.6.

The effective dielectric constant of the structure is calculated using the TL theory. It is found as [5]

$$\varepsilon_s = \left[\frac{2c}{a_p \omega} \arcsin \left(\frac{\omega}{\sqrt{2}\omega_m} \sqrt{1 - \frac{\omega_p^2}{\omega^2 + i\gamma_m \omega}} \right) \right]^2 \tag{3.1}$$

where ω_p and ω_m are defined as

$$\omega_p = \sqrt{\frac{1}{C_r L_r}}, \tag{3.2}$$

$$\omega_m = \sqrt{\frac{1}{C_r L_m}} \tag{3.3}$$

where L_m and C_r are the inductance and capacitence per unit length l_r of the transmission line respectively.

The inductance L_r of the metallic nano-hole rod is written as [5]

$$L_r = \frac{\mu_0 a_p}{2\pi} \left[\ln \left(\frac{2l_r}{r_r} \right) - \frac{3}{4} \right] \tag{3.4}$$

where μ_0 is the permeability.

Let us consider the transverse mode (TM) of the electromagnetic (EM) wave. The H field of the EM wave oscillates along the interface of the nano-hole array structure and dielectric (i.e. pyrex) substrate i.e. along y and z directions. The dispersion relations for the dielectric

substrate and nano-hole array structure are written as [5]

$$\begin{aligned} k_d &= \frac{\omega}{c}\sqrt{\varepsilon_d} \\ k_s &= \frac{\omega}{c}\sqrt{\varepsilon_s} \end{aligned} \tag{3.5}$$

where ε_d is the dielectric constant of the pyrex substrate and ε_s is given by eqn. (3.1). The EM wave propagates along z direction and decays in both slabs along x direction. Therefore, the TM wave is written as

$$\begin{aligned} H_{dy} &= Ae^{k_{dx}x}e^{-ik_z z}e^{-i\omega t} \qquad x<0 \\ H_{sy} &= Be^{-k_{sx}x}e^{-ik_z z}e^{-i\omega t} \qquad x>0 \end{aligned} \tag{3.6}$$

where A and B are the amplitude of the EM field inside the dielectric material and the nano-hole array structure respectively. Here k_{dx} and k_{sx} are the x-components of the wave vectors k_d and k_s respectively. The parameter k_z is the z-component of the wave vector for the TM mode in both the materials.

Using the boundary condition at the interface $x = 0$ and Bloch theorem, we get the following condition for SPP modes [5]

$$\frac{\left(k_z + \frac{n\pi}{a_p}\right)^2 - \left(\frac{\omega}{c}\right)^2 \varepsilon_s}{k_z^2 - \left(\frac{\omega}{c}\right)^2 \varepsilon_d} = \frac{\left(\frac{\omega}{c}\right)^4 \varepsilon_s^2}{\left(\frac{\omega}{c}\right)^4 \varepsilon_d^2} \tag{3.7}$$

Solving the above equation, we get the following expression of dispersion relation for SPP modes,

$$k_z = G_n(\omega), \tag{3.8}$$

$$G_n(\omega) = \frac{\left(\frac{n\pi}{a_p}\right)\varepsilon_d^2}{\varepsilon_s^2 - \varepsilon_d^2} \pm \sqrt{\left(\frac{\left(\frac{n\pi}{a_p}\right)\varepsilon_d^2}{\varepsilon_s^2 - \varepsilon_d^2}\right)^2 - \frac{\left(\frac{n\pi}{a_p}\right)^2 \varepsilon_d^2}{\varepsilon_d^2 - \varepsilon_s^2} + \frac{\left(\frac{\omega}{c}\right)^2 \varepsilon_s \varepsilon_d}{\varepsilon_s + \varepsilon_d}} \tag{3.9}$$

where $n = \sqrt{n_y^2 + n_z^2}$ is the quantum number. The numerical calculations are given in sec (3.3.1).

3.3 Polarizability of nano-hole array structure

The electric field component E_s inside the nano-hole array structure is given as

$$E_s = \mathrm{Im}(k_z)\ E_0 e^{-ik_d x} e^{-ik_z z} e^{-i\omega t} \tag{3.10}$$

where E_0 is the amplitude of the external EM wave. The polarization α_{pol} of the nano-hole structure is calculated from the above equation as [5],

$$\alpha_{pol} = \alpha_0\, \mathrm{Im}(k_z) \tag{3.11}$$

where $\alpha_0 = 4\pi\varepsilon_0 V_s$ and V_s is the volume of the nano-hole structure. The numerical calculations for polarizability is given in sec (3.3.1).

3.3.1 Numerical simulations

We have calculated the SPP energies numerically for samples A_1 using eqn. (3.9). Experimental parameters for sample A_1 are taken as $r_r = 50\ nm$, $l_r = 100\ nm$ and $a_p = 360\ nm$. The values of L_r, C_r and L_m appearing in theory were calculated as follows. Inductance was calculated from eqn. (3.4) and found to be $L_r = 45.8\ fH$. Capacitance was calculated from the experimental value of ω_p using eqn. (3.2) and found to be $C_r = 1.85\ aF$. The value of ω_m was taken as $\omega_m = 0.1\omega_p$ from the literature [6]. The value of $L_m$was computed to be $L_m = 4.58\ pH$. The dispersion relation for sample A_1, A_2 and A_3 are plotted in Fig. 3.2, 3.3 and 3.4 respectively as a function of energy and wave vector k_z. The

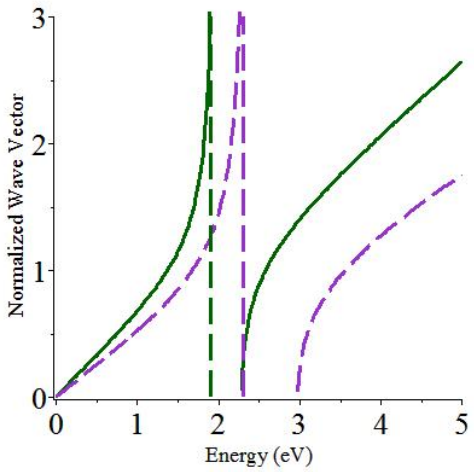

Figure 3.1: The SPP dispersion relation of the nano-hole array structure where the solid curve corresponds to $n = 0$ and the dashed curve represents $n = 1$ for sample A_1.

solid curve corresponds to the first Brillouin zone ($n = 0$) and the dashed curve represents the second Brillouin zone with $n = 1$. The SPP frequencies $\varepsilon_0^{sp}$and ε_1^{sp}can be calculated from Fig. 3.2 for sample A_1,when the wave vector k_z reaches infinity [7]-[8]. They were computed to be $\varepsilon_0^{sp} = 1.9eV$and $\varepsilon_1^{sp} = 2.3eV$ for $n = 0$ and $n = 1$, respectively for A_1. The wave vector is normalized to periodicity.Using the above eqn. (3.9), we have also calculated the SPPs for samples A_2 and A_3. The physical parameters for sample A_2 were $r_r = 60\ nm,\ l_r = 100\ nm$ and $a_p = 400\ nm,\ L_r = 36.3\ fH$,$C_r = 2.50\ aF$, and $L_m = 3.63\ pH$. The computed SPP energies were $\varepsilon_0^{sp} = 1.8eV$ and $\varepsilon_1^{sp} = 2.25eV$. Parameters for A_3 were $r_r = 70\ nm,\ l_r = 100\ nm$ and $a_p = 440\ nm,\ L_r = 26.3\ fH$,$C_r = 3.90\ aF$, and $L_m = 2.63\ pH$. The computed SPP energies were $\varepsilon_0^{sp} = 1.65eV$and $\varepsilon_1^{sp} = 2.11eV$.The normalized polarizability (α_{pol}/α_0) for sample A_1 was calculated from eqn. (3.11) and is plotted as a function of energy in Fig. 3.5. The decay rate is taken as γ_m =0.4 eV. Note that the polarizability curve has two peaks which correspond to $n = 0$ and $n = 1$.

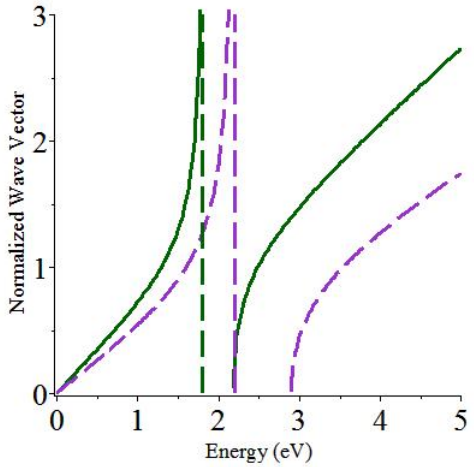

Figure 3.2: The SPP dispersion relation of the nano-hole array structure where the solid curve corresponds to $n = 0$ and the dashed curve represents $n = 1$ for sample A_2.

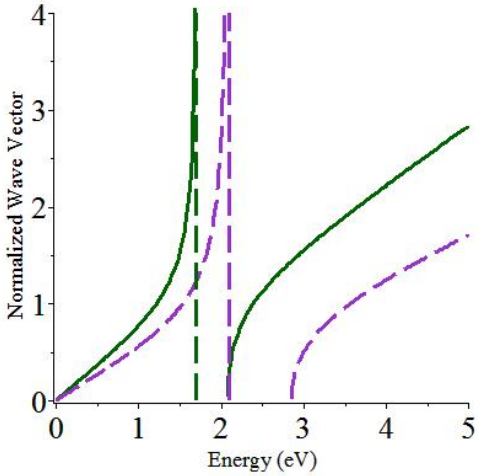

Figure 3.3: The SPP dispersion relation of the nano-hole array structure where the solid curve corresponds to $n = 0$ and the dashed curve represents $n = 1$ for sample A_3.

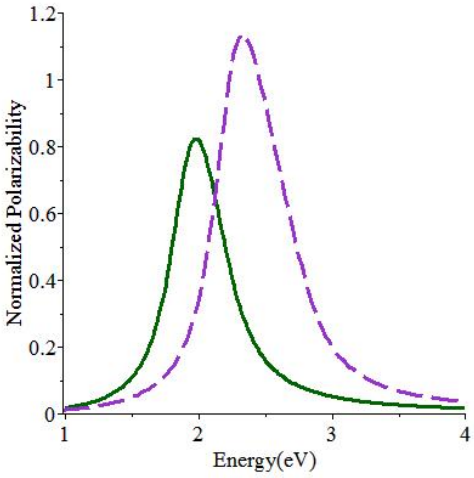

Figure 3.4: The plot of the normalized polarizability as a function of energy where the solid curve corresponds to $n = 0$ and the dashed curve represents $n = 1$ for sample A_1.

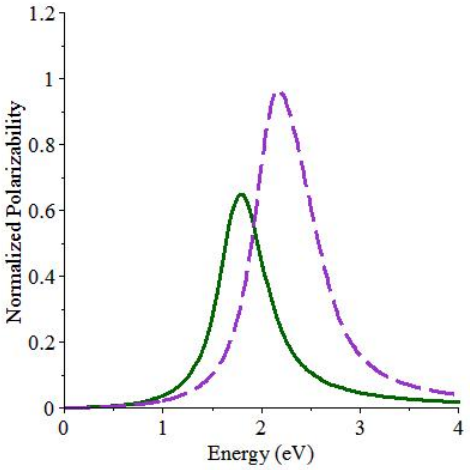

Figure 3.5: The plot of the normalized polarizability as a function of energy where the solid curve corresponds to $n = 0$ and the dashed curve represents $n = 1$ for sample A_3.

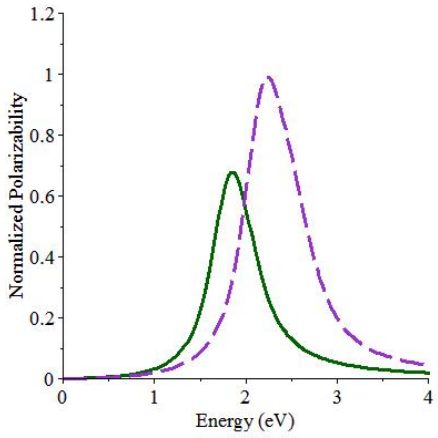

Figure 3.6: The plot of the normalized polarizability as a function of energy where the solid curve corresponds to $n = 0$ and the dashed curve represents $n = 1$ for sample A_2.

Locations of peaks in the polarizability plot give the SPP energies [7]-[8]. They are located at $\varepsilon_0^{sp} = 1.9eV$and $\varepsilon_1^{sp} = 2.3eV$. We have also calculated the SPPs using the polarizibility for sample A_2 and they are found as $\varepsilon_0^{sp} = 1.8eV$and $\varepsilon_1^{sp} = 2.25eV$. The normalized polarizability for sample A_2 was calculated as a function of energy and plotted in Fig. 3.6. Similarly for sample A_3 the SPP energies are found as $\varepsilon_0^{sp} = 1.65eV$and $\varepsilon_1^{sp} = 2.11eV$ and the normalized polarizability for sample A_3 was calculated as a function of energy and plotted in Fig. 3.7. Note that calculation of the SPP values from the polarizability method agree well with the estimates obtained with the SPP dispersion method. These SPP values were used to calculate the scattering cross section as described in the Results and Discussions section below.

3.4 Scattering cross section of nano-hole array structure

In this section, we calculate the scattering cross section of light from the NHA structure. The scattering cross section is defined in chapter 2 using the quantum Green's function method and quantum perturbation theory. The scattering cross section is calculated in [5]. The detailed derivation is provided in Appendix A. The expression for the scattering cross section is found as [5]

$$\left(\frac{d\sigma}{d\Omega}\right)_{spp} = \sum_n \frac{4d_n^2 G_n'(\varepsilon_n^{sp})}{\varepsilon_0 \hbar} \left(\frac{\Gamma_n}{(\varepsilon - \varepsilon_n^{sp})^2 + \Gamma_n^2}\right) \tag{3.12}$$

where $G_n'(\varepsilon_n^{sp})$ is the energy derivative of $G_n(\varepsilon)$ at $\varepsilon = \varepsilon_n^{sp}$. Here Γ_n is the line width (i.e. decay rate) of the n^{th} SPP eigen ket $|n\rangle$ and $d_n = \langle n| V_{int} |n\rangle$ is the matrix element of the dipole moment operator $\mathbf{d}$ induced by the EM field $\mathbf{E}$.

Similarly, the scattering cross section of light with bulk plasmon in the nano-hole structure is written as [5]

$$\left(\frac{d\sigma}{d\Omega}\right)_{pl} = \sum_n \frac{4d_{pl}^2 k_s k_s'(\varepsilon_p)}{\pi \varepsilon_0 \hbar} \left(\frac{\Gamma_{pl}}{(\varepsilon - \varepsilon_p)^2 + \Gamma_{pl}^2}\right) \tag{3.13}$$

where $k_s'(\varepsilon_p)$ is energy derivative of $k_s(\varepsilon)$ at $\varepsilon = \varepsilon_p$.Here Γ_{pl} is the line width (i.e. decay rate) of the plasmon state eigen d_{pl} is the matrix element of the dipole moment operator $\mathbf{d}$ induced by the EM field $\mathbf{E}$.

3.5 Results and Discussion

In this section we compare the theoretical results of the scattering cross section with experimental data obtained as described in section (2.7). The scattering cross section was calculated using eqn. (3.9) for all three samples A_1, A_2 and A_3.The experimental

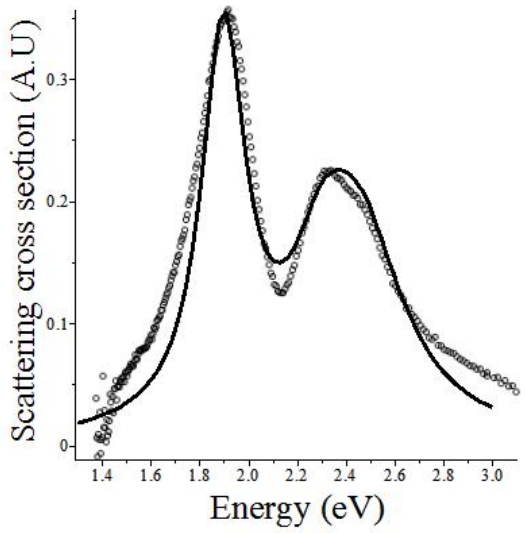

Figure 3.7: The scattering cross section in arbitrary units (A.U) for sample $A_1$is plotted as a function of energy (eV). Here the circles correspond to experimental data and the sold curve represents the theoretical calculations. The two peaks correspond to SPP modes.

transmission coefficient (i.e. scattering cross section) data for sample A_1 is shown in Fig. 3.8 and denoted by circles. The physical parameters of this sample are chosen as $r_r = 50\ nm$ and $a_p = 360\ nm$.Experimental values of the SPP decay rates (line width) and are not known in the literature. Therefore, we treat them as fitting parameters. When we used $\Gamma_0 = \Gamma_1 = 0.14eV$ for both the SPPs, we get a qualitative agreement between theory and the experiments. Results are not presented here. However, it is well known that each energy level has its own decay rate. It is well established that decay rates can control the widths and the heights of the scattering peaks. Therefore we have considered $\Gamma_0 \neq \Gamma_1$. Using $\Gamma_0 = 0.11\ eV$ and $\Gamma_1 = 0.15\ eV$, we have calculated the scattering cross section as a function of energy. The theoretical results are plotted as a solid line in Fig. 3.8. The spectrum of the scattering cross section has two peaks and they lie at $\varepsilon_0^{sp} = 1.9eV$and $\varepsilon_1^{sp} = 2.3eV$. Note that there is a good agreement between theory

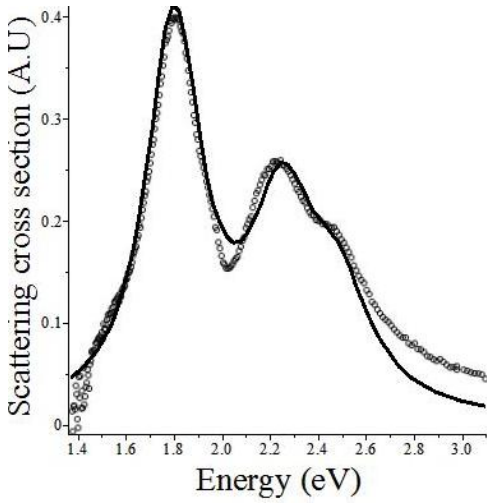

Figure 3.8: The scattering cross section in arbitrary units (A.U) for sample A_2 is plotted as a function of energy (eV). Here the circles correspond to experimental data and the sold curve represents the theoretical calculations. The two peaks correspond to SPP modes. The third hidden peak is due to bulk plasmon.

and experiment.Next, we calculated the scattering cross section for the second sample A_2. Sample A_2 had radius, $r_r = 60\ nm$ and periodicity, $a_p = 400\ nm$.The theoretical results along with experimental results are plotted in Fig. 3.9. Circles denote experimental data points and the solid curve represents theoretical results. Note that the scattering cross section spectrum has three peaks. The first two peaks correspond to $n = 0$ and $n = 1$ SPP modes. The first peak is located at the SPP energy of $\varepsilon_0^{sp} = 1.8eV$ and the second peak is located at the SPP energy of $\varepsilon_1^{sp} = 2.25eV$. The decay rate of two SPP modes were chosen as $\Gamma_0 = 0.14\ eV$ and $\Gamma_1 = 0.16\ eV$. The third peak it is located at $\varepsilon_{pl} = 2.45eV$. The last peak is not due to the SPP modes but corresponds to the bulk plasmon of the nano-hole structure. The bulk plasmon peak is apparent as a shoulder on the second peak for both the experiment and theoretical prediction shown in Fig. 3.9. It is because that the decay rate of plasmons due to the plasmon-phonon scattering in metals is large. The

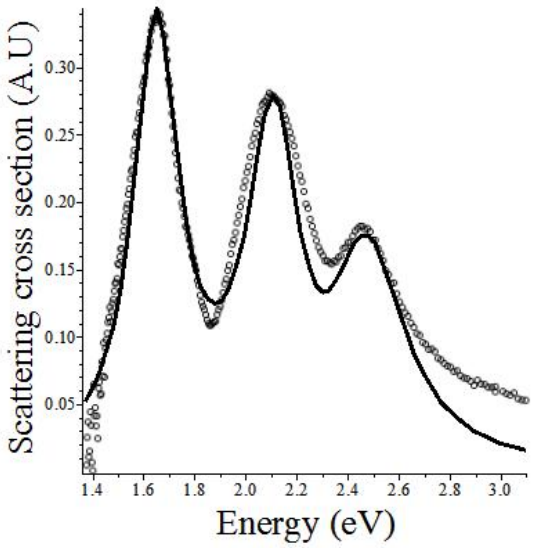

Figure 3.9: The scattering cross section in arbitrary units (A.U) for sample $A_1$is plotted as a function of energy (eV). Here the circles correspond to experimental data and the sold curve represents the theoretical calculations. The two peaks correspond to SPP modes. The third peak is due to bulk plasmon.

value of Γ_{pl} is taken as $\Gamma_{pl} = 0.17\ eV$. Note, that again there was a good agreement between theory and experiment.Finally we calculated the scattering cross section for the third sample, A_3. For sample A_3, the periodicity and radius of the NHA structure was $r_r = 70\ nm$ and $a_p = 440\ nm$ respectively. Experimental data are shown in Fig. 3.10 with circles. Note that the spectrum has three peaks. The first two peaks corresponded to the SPP modes and the third peak was due to the bulk plasmon since it was located at $\varepsilon_{pl} = 2.45eV$. The bulk plasmon peak also appeared for sample A_2 at the same location. The decay rate of two SPP modes were chosen as $\Gamma_0 = 0.11\ eV$ and $\Gamma_1 = 0.13\ eV$ and the decay rate for the bulk plasmon is taken as $\Gamma_{pl} = 0.19\ eV$. Using these values, we calculated the scattering cross section as function of energy, which are plotted as solid curves in Fig. 3.10 along with experimental results (open circles). The first peak corresponded to the SPP

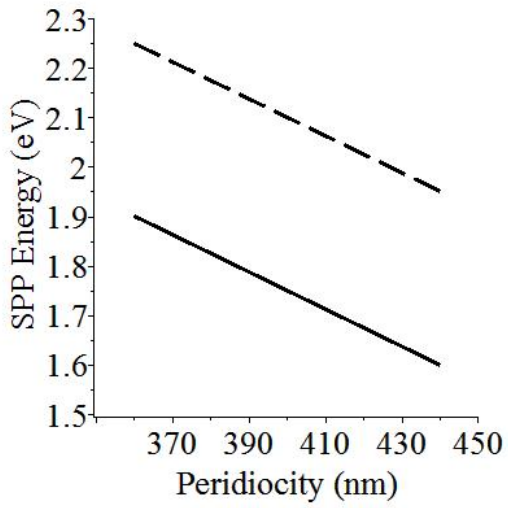

Figure 3.10: The SPP energy is plotted as a function of the periodicity of the holes, where solid curve corresponds to $n = 0$ and the dashed curve corresponds to $n = 1$. Here we have fixed the raius $r_r = 50nm$.

mode $\varepsilon_0^{sp} = 1.65eV$ and second peak belonged to the SPP mode $\varepsilon_1^{sp} = 2.11eV$. As with the previous two samples, there was a good agreement between theory and experiment.From Figs. 3.8-3.10 one can also find that the location of the SPP modes can be changed by modifying the periodicity of the nano-hole structure. To clarify this point we have plotted the SPP modes and as a function of periodicity in Fig. 3.11 for a fixed nano-hole radius. The solid and dotted lines represents and respectively. Note that as the periodicity increases the energy location of the SPP modes also decreases. This is an interesting finding which is consistent with our earlier simulation and experimental results [9]. The consistency of the overall findings suggest that the theory may be useful for designing and potentially optimizing the optical characteristics of a NHA structure based on its material and geometry properties without the need for lengthy simulations.

3.6 Conclusion

We have investigated the scattering cross section of light through metallic nano-hole array structures. The scattering cross section of the nano-hole array structure was calculated for three different samples with different nano-hole radii and periodicity. The dispersion relation and effective dielectric constant were calculated by using the TL theory. The SPPs were calculated by the transfer matrix method. We have found that the energies of the SPPs are quantized and systems can have several SPPs depending on the radius and periodicity of the structures. A good agreement between the theory and experimental work has also been achieved. It is proposed that the theory could be used to optimize nano sensors for medical and engineering applications.

Bibliography

[1] M. Achermann, J. Phys. Chem. Lett. 1, 2837 (2010).

[2] M. Singh, D. Schindel and A. Hatef, App. Phys. Lett. 99, 181106(2011).

[3] M. Singh, C. Racknor and D. Schindel , App. Phys. Lett. 101, 051115(2012).

[4] J. Cox, M. Singh, C. D. Bilderling and A. V. Bragas, Adv. Optical Mater. 1, 460(2013).

[5] T. W. Ebbesen, H. J. Lezec, H. F. Ghaemi, T. Thio and P. A. Wolf , Nature 391, 667 (1998).

[6] M. R. Singh, M. Najiminaini, S. Balakrishnan and J. J. L. Carson, J. Appl. Phys. 117, 184302 (2015).

[7] L. Solymar and E. Shamonina, *Waves in Metamaterials*, Oxford University Press, Oxford (2009)

[8] Mahi R. Singh, *Electronic, Photonic, Polaritonic, and Plasmonic Materials***,** Willey Custom, Toronto (2014).

[9] L. Novotony, *Principles of Nano-Optics*, 2nd Ed., Cambridge University Press (2012).

[10] M. Najiminaini, F. Vasefi, B. Kaminska, and J. J. L. Carson, Opt. Express 18 (21), 22255 (2010).

Chapter 4

Transmission coefficient of light in nano-hole array structures

In the previous chapter, the scattering cross section of light in nano-hole array (NHA) structure on a pyrex susbtrate for normal angle of incidence was calculated. It was found that the scattering cross section was dependent on the periodicity of the NHA structure. In this chapter, we investigate the dependence of transmission coefficient of light on the angle of incidence. We employ quantum density matrix method to calculate the transmission coefficient.

4.1 Introduction

The nano-hole array struture fabricated in a thin metal film on pyrex substrate allow incident light to couple with surface plasmon present at the metal-dielectric interface on one side of the metal and decouple on the other side of the film [1]-[3]. This mechanism

results in extraordinary optical transmission (EOT) of light. The EOT property of NHA has opened up new possibilities for wide range of applications such as surface plasmon resonance (SPR) sensing, surface enhanced Raman scattering (SERS).

In this chapter, we have calculated the transmission coefficient of light as a function of angle of the incident light with respect to the normal to the surface of the NHA. It is found that as the angle of incidence is increased from zero the number of peaks in the spectrum increases. To explain the experimental results, we have derived the angle dependence expression for the SPPs using the transfer matrix method and Bloch theorem. The transmission coefficient is calculated using the quantum mechanical density matrix method. In this method, one uses the average of an operator on wave functions of the system as well as the statistical ensemble of the system. In this theory the correlation and coherence effects between SPP modes are included automatically. On the other hand, it is very difficult to include the above effects in the quantum scattering theory [4]. We considered metallic nano-hole array structure as plasmonic metamaterial [5]. We have found that the energies of SPPs are quantized and the system can have several SPPs depending on the angle of incidence. This theory can be used to fabricate better performing NHA device.

4.2 Theoretical formalism

4.2.1 Surface Plasmon Polaritons

The nano-hole array structure slab is located above the dielectric material slab which is made of Pyrex. The interface between the nano-hole structure and dielectric materials lies at $x = 0$. A schematic diagram of the NHA is shown in Fig. 4.1. where nano-

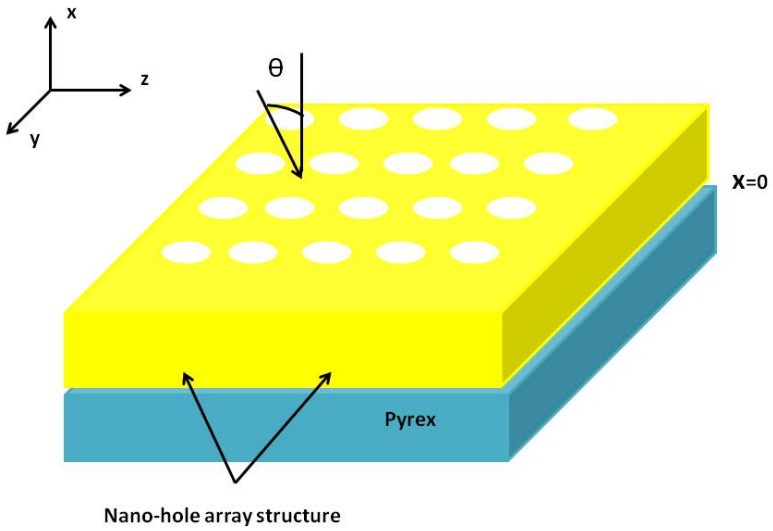

Figure 4.1: A schematic diagram of the nano-hole structure. The light is incident with an angle θ.

holes are arranged periodically in the $y-z$ plane in a cubic lattice structure. The radius and length of nanohole rods are taken as r_r and l_r, respectively. The periodicity of the NHA structure along z and y directions is taken as L_z and L_y, respectively.An electromagnetic (EM) wave with wave vector $\mathbf{k}$ is applied to the NHA structure and it makes an angle θ with respect to x axis. Hence the components of wave vector $\mathbf{k}$ in the cartesian and cylindrical coordinates are related as $k_x = k\cos\theta$, $k_y = k\sin\theta\sin\phi$ and $k_z = k\sin\theta\cos\phi$. The dielectric constant of Pyrex substrate is denoted as ε_d and is taken as $\varepsilon_d = 2.17$. The refractive index of the NHA structure is calculated in reference [4] .

The wave vectors of the EM wave propagating in the NHA structure and the substrate are

denoted as k_s and k_d, respectively. Their x-components are expressed as

$$k_{dx} = \sqrt{\left(k_z^2 + k_y^2\right) - \left(\frac{\omega}{c}\right)^2 \varepsilon_d} \tag{4.1}$$

$$k_{sx} = \sqrt{\left(k_z^2 + k_y^2\right) - \left(\frac{\omega}{c}\right)^2 \varepsilon_s} \tag{4.2}$$

The nano-hole array structure is periodic in z and y direction. According to the band structure theory and Bloch theorem the frequency of the EM wave propagating in the periodic structure must satisfy the periodicity condition [7] as

$$\omega(k_z, k_y) = \omega\left(k_z + \frac{2n_z\pi}{L_z}, k_y + \frac{2n_y\pi}{L_y}\right) \tag{4.3}$$

where n_z and n_y are integers.

To investigate the SPP modes in the nano-hole array structure, we apply Maxwell's equations at the metal-Pyrex interface. It is well known that SPPs exist only for TM polarization so the Maxwell's equation for TM modes is [6]

$$\frac{\partial^2 H_{sy}}{\partial x^2} + \frac{\partial^2 H_{sy}}{\partial y^2} + \frac{\partial^2 H_{sy}}{\partial z^2} = \left(\frac{\omega}{c}\right)^2 \varepsilon_s H_{sy} \tag{4.4}$$

$$\frac{\partial^2 H_{dy}}{\partial x^2} + \frac{\partial^2 H_{dy}}{\partial y^2} + \frac{\partial^2 H_{dy}}{\partial z^2} = \left(\frac{\omega}{c}\right)^2 \varepsilon_s H_{dy} \tag{4.5}$$

The solutions to the above equations in the half space yields

$$H_{sy} = A_s e^{-k_{sx}x} e^{-ik_y y} e^{-ik_z z} \qquad x > 0 \tag{4.6}$$

$$H_{dy} = A_d e^{-k_{dx}x} e^{-ik_y y} e^{-ik_z z} \qquad x < 0 \tag{4.7}$$

where A_s and A_d are the amplitudes of EM field in the NHA structure and substrate respectively.

Using the boundary condition at the interface $x = 0$ and Bloch theorem [7], we get the

following expression of the SPPs

$$\left(k_z + \frac{2n_z\pi}{L_z}\right)^2 + \left(k_y + \frac{2n_y\pi}{L_y}\right)^2 = \left(\frac{\omega}{c}\right)^2 \left(\frac{\varepsilon_s\varepsilon_d}{\varepsilon_s + \varepsilon_d}\right) \tag{4.8}$$

Expressing the above expression in the cylindrical polar coordinates we get

$$\left(\frac{\omega}{c}\sin\theta\cos\phi + \frac{2n_z\pi}{L_z}\right)^2 + \left(\frac{\omega}{c}\sin\theta\sin\phi + \frac{2n_y\pi}{L_y}\right)^2 = \left(\frac{\omega}{c}\right)^2 \left(\frac{\varepsilon_s\varepsilon_d}{\varepsilon_s + \varepsilon_d}\right) \tag{4.9}$$

The above expression can be further simplified by putting $\phi = 0$ without loss of physics as

$$\left(\frac{\omega}{c}\sin\theta + \frac{2n_z\pi}{L_z}\right)^2 + \left(\frac{2n_y\pi}{L_y}\right)^2 = \left(\frac{\omega}{c}\right)^2 \left(\frac{\varepsilon_s\varepsilon_d}{\varepsilon_s + \varepsilon_d}\right) \tag{4.10}$$

Here we consider the periodicity of the NHA structure to be same in both the directions and is taken as a_p.

According to eqn. (4.10), energy is quantized and has quantum numbers n_z and n_y.We denote the quantized energy as ε_n and its quantized states as $|n\rangle$.

4.2.2 Transmission coefficient: Density Matrix Method

In the previous section, we found that the SPPs in nano-hole array structure are in quantized states denotes as $|n\rangle$. The ground state of the SPP system has energy ε_0 with state $|0\rangle$. The next excited state is writen as $|n\rangle$ with energy ε_n, where $n = 1, 2, 3, 4, 5$.

The expression for transmission coefficient due to the transitions $|n\rangle \longleftrightarrow |0\rangle$ is derived in chapter 2 and it is given as,

$$\begin{aligned} \alpha_{trans} &= \sum_n \alpha_{0n}\,\mathrm{Im}\left(\rho_{on}\right) \\ \alpha_{0n} &= \frac{\mu_{0n}\varepsilon_p}{\hbar c E_p} \end{aligned} \tag{4.11}$$

where ε_p and E_p are the energy and amplitude of the EM field respectively. Here μ_{0n} is called as the dipole element between the states $|0\rangle$ and $|n\rangle$. The density matrix elements

$\rho_{0n} = \langle 0| \rho |n\rangle$ appearing in the above expression are numerically obtained from the following expressions for density matrix elements. The detailed derivation is provided in Appendix B.

$$
\begin{aligned}
\frac{d\rho_{22}}{dt} &= -2\gamma_2\rho_{22} - i\left(\Omega_{02}\right)\rho_{02} - i\left(\Omega_{02}\right)^*\rho_{20} \\
\frac{d\rho_{20}}{dt} &= -(\frac{\gamma_2}{2} + i\Delta_{02})\rho_{20} - i\left(\Omega_{02}\right)\left(\rho_{22} - \rho_{00}\right) - i(\Omega_{01})\rho_{21} - i(\Omega_{03})\tilde{\rho_{23}} - i(\Omega_{04})\tilde{\rho_{24}} - i(\Omega_{05})\tilde{\rho_{25}} \\
\frac{d\rho_{11}}{dt} &= -2\gamma_1\rho_{11} - i\left(\Omega_{01}\right)\rho_{01} - i\left(\Omega_{01}\right)^*\rho_{10} \\
\frac{d\rho_{10}}{dt} &= -(\frac{\gamma_1}{2} + i\Delta_{01})\rho_{10} - i\left(\Omega_{01}\right)\left(\rho_{11} - \rho_{00}\right) - i(\Omega_{02})\rho_{12} - i(\Omega_{03})\tilde{\rho_{13}} - i(\Omega_{04})\tilde{\rho_{14}} - i(\Omega_{05})\tilde{\rho_{15}} \\
\frac{d\rho_{21}}{dt} &= -[\frac{(\gamma_2 + \gamma_1)}{2} + i(\Delta_{02} - \Delta_{01})]\rho_{21} + i\left(\Omega_{02}\right)\rho_{01} - i\left(\Omega_{01}\right)^*\rho_{20} \\
\frac{d\rho_{33}}{dt} &= -2\gamma_3\rho_{33} - i\left(\Omega_{03}\right)\rho_{03} - i\left(\Omega_{03}\right)^*\rho_{30} \\
\frac{d\rho_{30}}{dt} &= -(\frac{\gamma_3}{2} + i\Delta_{03})\rho_{30} - i\left(\Omega_{03}\right)\left(\rho_{33} - \rho_{00}\right) - i(\Omega_{01})\rho_{31} - i(\Omega_{02})\tilde{\rho_{32}} - i(\Omega_{04})\tilde{\rho_{34}} - i(\Omega_{05})\tilde{\rho_{35}} \\
\frac{d\rho_{32}}{dt} &= -[\frac{(\gamma_3 + \gamma_2)}{2} + i(\Delta_{03} - \Delta_{02})]\rho_{32} + i\left(\Omega_{03}\right)\rho_{02} - i\left(\Omega_{02}\right)^*\rho_{30} \\
\frac{d\rho_{44}}{dt} &= -2\gamma_4\rho_{44} - i\left(\Omega_{04}\right)\rho_{04} - i\left(\Omega_{04}\right)^*\rho_{40} \\
\frac{d\rho_{40}}{dt} &= -(\frac{\gamma_4}{2} + i\Delta_{04})\rho_{40} - i\left(\Omega_{04}\right)\left(\rho_{44} - \rho_{00}\right) - i(\Omega_{01})\rho_{41} - i(\Omega_{02})\tilde{\rho_{42}} - i(\Omega_{03})\tilde{\rho_{43}} - i(\Omega_{05})\tilde{\rho_{45}} \\
\frac{d\rho_{43}}{dt} &= -[\frac{(\gamma_4 + \gamma_3)}{2} + i(\Delta_{04} - \Delta_{03})]\rho_{43} + i\left(\Omega_{04}\right)\rho_{03} - i\left(\Omega_{03}\right)^*\rho_{40} \\
\frac{d\rho_{55}}{dt} &= -2\gamma_5\rho_{55} - i\left(\Omega_{05}\right)\rho_{05} - i\left(\Omega_{05}\right)^*\rho_{50} \\
\frac{d\rho_{50}}{dt} &= -(\frac{\gamma_5}{2} + i\Delta_{05})\rho_{50} - i\Omega_{05}\left(\tilde{\rho_{55}} - \tilde{\rho_{00}}\right) - i(\Omega_{01})\rho_{51} - i(\Omega_{02})\tilde{\rho_{52}} - i(\Omega_{03})\tilde{\rho_{53}} - i(\Omega_{04})\tilde{\rho_{54}} \\
\frac{d\rho_{54}}{dt} &= -[\frac{(\gamma_5 + \gamma_4)}{2} + i(\Delta_{05} - \Delta_{04})]\rho_{54} + i\left(\Omega_{05}\right)\rho_{04} - i\left(\Omega_{04}\right)^*\rho_{50}
\end{aligned}
$$

Here $\Delta_{ij} = \omega_{ij} - \omega$ is called the probe field tunings. Physical quantitites $\gamma_1, \gamma_2, \gamma_3, \gamma_4$ and γ_5 are the spontaneous decay rates of the levels $|1\rangle, |2\rangle, |3\rangle, |4\rangle$ and $|5\rangle$. Here Ω_{0n} is called the Rabi frequency associated with the transition $|n\rangle \longleftrightarrow |0\rangle$.

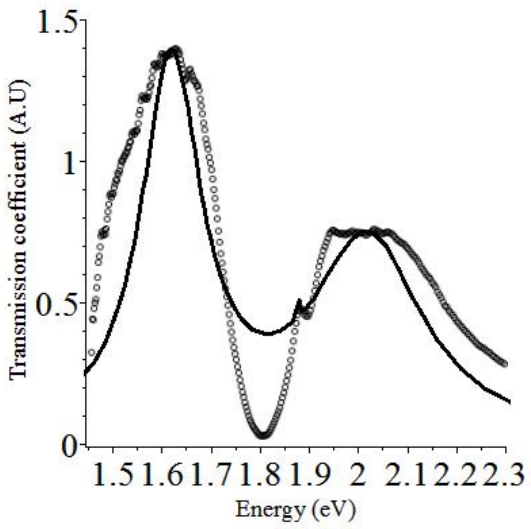

Figure 4.2: Transmission coefficient in arbitrary units (A.U) as a function of energy (eV) for $\theta = 0^\circ$. Here the circles represent the experimental data and the solid curve corresponds to theoretical calculations.

4.3 Results and Discussion

In this section, we compare our theoretical transmission coefficient with experimental data. The transmission coefficient was calculated for $\theta = 0^\circ,\ \theta = 5^\circ$ and $\theta = 12^\circ$. We have calculated the SPP energies numerically for three different angles of incidence viz. $\theta = 0^\circ,\ \theta = 5^\circ$ and $\theta = 12^\circ$ using eqn. (4.10). Experimental parameters are taken as $r_r = 140\ nm,\ l_r = 100\ nm$ and $L_y = L_z = 440\ nm$. The values of L_r, C_r and L_m appearing in theory were calculated as follows. Inductance was calculated from eqn. (3.4) and found to be $L_r = 21.8\ fH$. Capacitance was calculated from the experimental value of ω_p using eqn. (3.2) and found to be $C_r = 1.10\ aF$. The value of $\omega_m = 0.1\omega_p$was taken from the literature [8]. The value of L_m was computed to be $L_m = 2.18\ pH$. The experimental transmission coefficient for $\theta = 0^\circ$ is shown in Fig. 4.2 and is de-

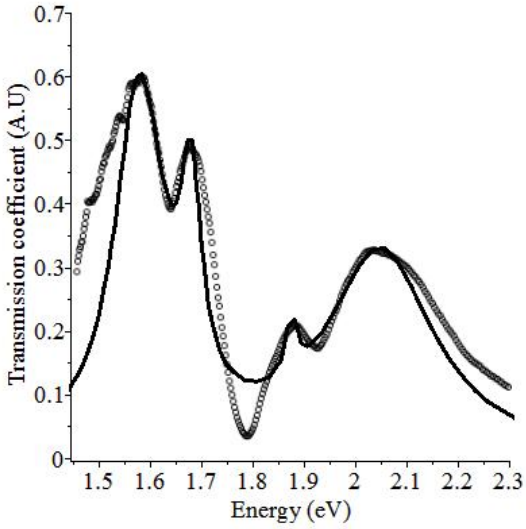

Figure 4.3: Transmission coefficient in arbitrary units (A.U) as a function of energy (eV) for $\theta = 5^\circ$. Here the circles represent the experimental data and the solid curve corresponds to theoretical calculations

noted by circles. The SPP decay rates used are $\Gamma_1 = 0.13\ eV$, $\Gamma_2 = 0.02\ eV$ and $\Gamma_3 = 0.25\ eV$. The SPP energies were computed to be $\varepsilon_1 = 1.62\ eV$, $\varepsilon_2 = 1.88\ eV$ and $\varepsilon_3 = 2.05\ eV$ corresponding to $(n_z, n_y) = (-1, 0), (-1, 1)$ and $(2, 0)$ modes respectively. The transmission coefficient was calculated as a function of energy and it is plotted in Fig. 4.2. Next we calculated the SPP energies for $\theta = 5^\circ$ and they were computed to be $\varepsilon_1 = 1.58\ eV$ corresponds to $(n_z, n_y) = (-1, 0), \varepsilon_2 = 1.68\ eV$ corresponds to $(n_z, n_y) = (1, 0)$, $\varepsilon_3 = 1.87\ eV$, corresponds to $(n_z, n_y) = (-1, 1)$ and $\varepsilon_4 = 2.04\ eV$ corresponds to $(2, 0)$ modes. The theoretical calculations along with the experimental results are plotted in Fig. 4.3. The decay rates of SPP modes were chosen as $\Gamma_1 = 0.03\ eV$, $\Gamma_2 = 0.008\ eV$, $\Gamma_3 = 0.002\ eV$ and $\Gamma_4 = 0.04\ eV$. Note that there was a good agreement between theory and experiments. Finally, we calculated the transmission coefficient for $\theta = 12^\circ$. The experimental and theoretical transmission

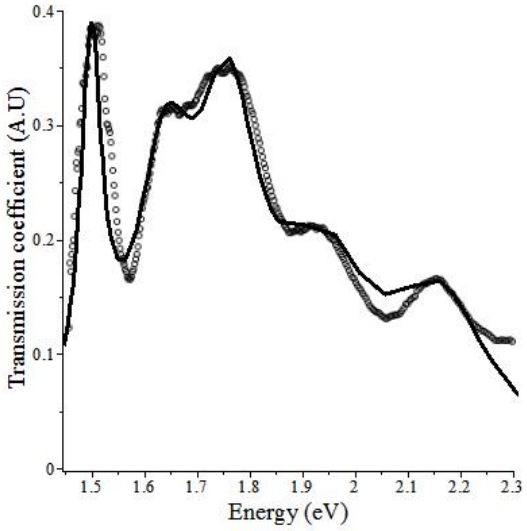

Figure 4.4: Transmission coefficient in arbitrary units (A.U) as a function of energy (eV) for $\theta = 12^{\circ}$. Here the circles represent the experimental data and the solid curve corresponds to theoretical calculations.

is plotted in Fig. 4.4. The transmission spectrum has 5 peaks. The SPP energies were computed to be $\varepsilon_1 = 1.5\ eV$ which corresponds to $(n_z, n_y) = (-1, 0)$. The second peak is located at $\varepsilon_2 = 1.65eV$ corresponding to $(n_z, n_y) = (0, 1)$ and the other peaks $\varepsilon_3 = 1.76\ eV$, $\varepsilon_4 = 1.94\ eV$ and $\varepsilon_5 = 2.16eV$ correspond to $(n_z, n_y) = (1, 0)$, $(-1, 1)$ and $(2, 0)$ modes respectively. The SPP decay rates were chosen as $\Gamma_1 = 0.05\ eV$, $\Gamma_2 = 0.14\ eV$, $\Gamma_3 = 0.15\ eV$, $\Gamma_4 = 0.2\ eV$ and $\Gamma_5 = 0.23\ eV$. Note that there is a good agreement between theory and experiment.From Figs. 4.2-4.4, It is found that the location of SPP modes can be changed by angle of incidence of the photon. To clarify this point, we have plotted the SPP modes as a function of angle in Fig. 4.5. The dashed curve corresponds to $(1, 0)$ mode, dotted curve corresponds to $(-1, 0)$ mode, the dash-dotted curve corresponds to $(2, 0)$ mode. Note that as angle of incidence increases, the energies of the SPP modes $(-1, 0)$ decreases whereas the energies of $(1, 0)$ and $(2, 0)$ modes increase. One can find that

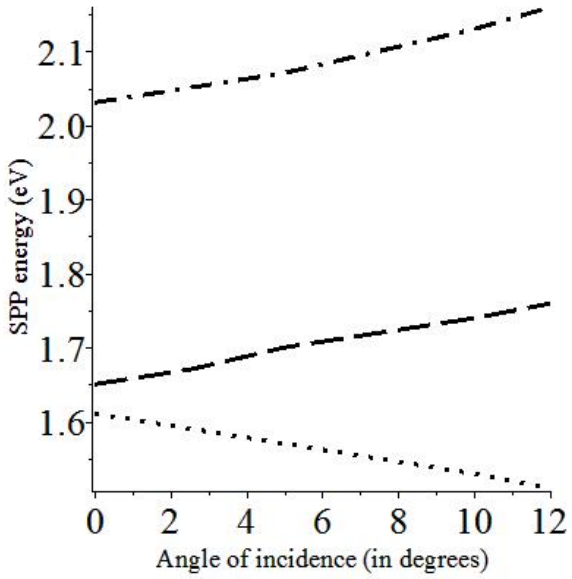

Figure 4.5: The SPP energy as a function of angle of incidence for various modes.

the transmission coefficient also decreases with the increase in angle of incidence. This is an interesting finding which is consistent with the experiment.

4.4 Conclusion

The transmission coefficient of light through metallic nano-hole array structure was investigated theoretically. The transmission coefficient was measured for three different angles of incidence. We have also found that the energies of SPP are quantized and a NHA structure can have many SPPs. A theory of transmission coefficient based on quantum density matrix was developed. A good agreement between the theory and experiment was observed.

Bibliography

[1] T. W. Ebbesen, H. J. Lezec, H. F. Ghaemi, T. Thio and P. A. Wolf, Nature 391, 667 (1998).

[2] H. F. Ghaemi, T. Thio, D. E. Grupp, T. W.W Ebbesen and H. J. Lezec, Phys. Rev. B 58(11), 6779 (1998).

[3] L. Martin- Moreno, F. J. Garcia-Vidal, H. J. Lezec, K. M. Pellerin, T. Thio, J. B. Pendry and T. W. Ebbesen, Phys. Rev. Lett., 86(6), 1114 (2001).

[4] M. R. Singh, M. Najiminaini, S. Balakrishnan and J. J. L. Carson, J. Appl. Phys. 117 , 184302 (2015).

[5] C. Carloz and T. Itoh, Electromagnetic Metamaterials (Wiley Interscience, Hoboken, New Jersey, 2006).

[6] Mahi R. Singh, Electronic, Photonic, Polaritonic, and Plasmonic Materials, Willey Custom, Toronto (2014).

[7] C. Kittel, Introduction to Solid State Physics, 7th Ed., John Wiley & Sons, Inc.(1996).

[8] L. Solymar and E. Shamonina, Waves in Metamaterials (Oxford University Press, Oxford (2009)).

Chapter 5

Transmission and Reflection in couplers made from nano-hole array structure[1]

In the previous chapter, the transmission coefficient of NHA structure was calculated for different angles of incidence. In this chapter, we have studied the reflection and transmission coefficient of the nano-hole array coupler.

5.1 Introduction

A waveguide is a device or structure that guides electromagnetic waves or sound waves. The electromagnetic waveguides used at optical frequencies, also called as optical waveguides, are typically made up of dielectric materials with high index of refraction and

[1]Reproduced with permission from M. R. Singh and Shankar Balakrishnan, AIP Conf. Proc., vol 1590, 271 (2014). Copyright 2014, AIP Publishing LLC.

are surrounded by a material with lower refractive index [1]-[5]. The waveguides are used to transmit light and signals for long distances with high signal rate (e.g. optical fibers) and are also used in intergrated optical circuits [6]. Each waveguide has modes that propagate at different velocities. If the two waveguides are brought closer to each other, the optical modes of each waveguide interact with each other. This mechanism is called directional coupling and the devices are called directional couplers. Waveguide directional couplers perform a number of useful functions in optical communications , including power division, power coupling and switching [7]. These structures may be fabricated from compound-glass fibres, metals and semiconductor materials [1]-[3]. More recently, nanowires and couplers made from photonic crystals and polaritonic materials have also been studied [4]-[5].

In this chapter, we have studied the transmission and reflection in nano-hole array (NHA) couplers. They are fabricated from the metallic nano-hole array structure. The NHA structure is embedded between two dielectric waveguides. A schematic diagram of the coupler is shown in Fig. 5.1. Using the transfer matrix method and coupled mode theory, expressions for the reflection and transmission coefficients of electromagnetic wave propagating in waveguides have been obtained. We consider an electromagnetic (EM) wave that is incident on one of the waveguides, travelling to the left. In the second waveguide, a reflected EM wave appears, which is travelling to the right. This occurs because the two EM waves couple with each other via the NHA structure due to the dipole coupling.

Numerical simulations were performed on the reflection and transmission coefficients for the coupler. For the numerical simulations we have considered that both waveguides consist of silica, while the NHA structure is made from silver film. It is ob-

served that for certain energies the EM wave is totally reflected by the coupler, and for other energies light is totally transmitted. We have considered that due to the external stress and pressure the lattice constant (or periodicity) of the NHA structure is modified. We found that changing the periodicity of the NHA structure, the transmission and reflection properties of the coupler are modified. In other words the present findings can be used to make new types optical sensors

5.2 Transmission and Reflection in metallic NHA couplers

Let us consider two waveguides A and B. An NHA structure is embedded between two waveguides. The periodicity of the NHA structure is taken as a_p. A schematic diagram of the coupler is shown in Fig. 5.1.The waveguides are oriented along the z-direction. Let $n^2(x,y)$ be the refractive index distribution of the NHA coupler. It is written as [7]

$$\begin{aligned} n^2(x,y) &= n_A^2, \quad waveguide\ A \\ n^2(x,y) &= n_B^2, \quad waveguide\ B \\ n^2(x,y) &= n_s^2, \quad NHA\ structure \end{aligned} \tag{5.1}$$

where n_s is the refractive index of NHA structure defined in the ref [8]. For the purpose of mathematical convenience in the mode coupling, we define

$$\begin{aligned} \Delta n_A^2(x,y) &= n_A^2 - n_s^2 \\ \Delta n_B^2(x,y) &= n_B^2 - n_s^2 \end{aligned} \tag{5.2}$$

The index profile of the NHA coupler can now be written as [7]

$$n^2(x,y) = n_s^2(x,y) + \Delta n_A^2(x,y) + \Delta n_B^2(x,y) \tag{5.3}$$

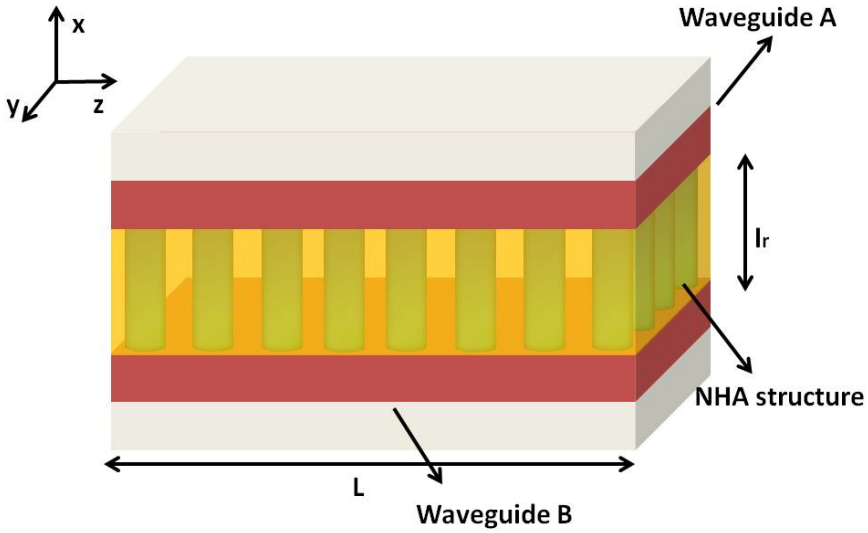

Figure 5.1: A schematic diagram of NHA coupler made up of silica waveguides and silver NHA structure.

The Maxwell's equation for the NHA coupler is given by

$$\left(\frac{\partial^2}{\partial x^2}+\frac{\partial^2}{\partial y^2}+\frac{\partial^2}{\partial z^2}+\left(\frac{\omega}{c}\right)^2\left[n_s^2(x,y)+\Delta n_A^2(x,y)+\Delta n_B^2(x,y)\right]\right)\mathbf{E}=0 \tag{5.4}$$

The electric field of a general wave propagation in the NHA coupler is written as [7]

$$\mathbf{E}(x,y,z)=A(z)E_a(x,y)e^{-ik_Az}+B(z)E_b(x,y)e^{-ik_Bz} \tag{5.5}$$

where $\mathbf{E}_A(x,y,z)=A(z)E_a(x,y)e^{ik_Az}$ and $\mathbf{E}_B(x,y,z)=B(z)E_b(x,y)e^{ik_Bz}$ are the modes of propagation of the individual waveguides A and B respectively. Here z dependence of the amplitudes $A(z)$ and $B(z)$ in waveguide A and B reflect the coupling of normal modes and, k_A and k_B are the the propagating wave vectors in wave guide A and B respectively. The modes form a complete orthogonal set and obey the orthonormalization relation [7]

$$\frac{\beta_m}{2\omega}\int\int E_m.E_n^*dx\ dy=\delta_{mn} \tag{5.6}$$

where m and $n = a, b$.

It's a well-known fact that coupling between two waveguides can be made highly efficient and frequency selective provided a periodic dielectric perturbation is introduced between the waveguides. We introduced a periodic metallic NHA structure with short-period between the wavguides A and B. This type of coupling which involves short-period (or high frequency) structure is called as contradirectional coupling and the coupler is called as contradirectional coupler [7].

Now the electric field of the optical propagation in this case is written as

$$E(x, y, z) = A(z)E_a(x, y)e^{-ik_A z} + B(z)E_b(x, y)e^{ik_B z} \tag{5.7}$$

Note that the mode in waveguide B is propagating along the $-z$ direction.

Putting eqn (5.7) into eqn (5.4) and assuming that the amplitude varies slowly over z,the Maxwell's equation reduces to [7]

$$\begin{aligned} \frac{dA}{dz} &= -i\kappa_{ab}Be^{-i(\Delta k)z} \\ \frac{dB}{dz} &= -i\kappa_{ba}Be^{i(\Delta k)z} \end{aligned} \tag{5.8}$$

where $\Delta k = \frac{\omega}{c}(n_A + n_B) - \frac{\pi}{a_p}$ is called as a phase factor. Here κ_{ab} and κ_{ba} are called as coupling constant. They are defined as [7]

$$\kappa_{ab} = \frac{\omega}{4}\varepsilon_0 \int\int E_a^{\star}.\Delta n_A^2(x, y)E_b \, dx \, dy \tag{5.9}$$

$$\kappa_{ba} = \frac{\omega}{4}\varepsilon_0 \int\int E_b^{\star}.\Delta n_B^2(x, y)E_a \, dx \, dy \tag{5.10}$$

Since we consider the waveguides to be identical, the two coupling coefficients form a conjugate pair $\kappa_{ba} = \kappa_{ab}^* = \kappa_T$.

The solutions to eqn. (5.8) for the contradirectional coupling subject to $B(L) = 0$ is written as [7]

$$A(z) = e^{i\Delta kz}\frac{\Omega\cosh\Omega(L-z) + i(\Delta k)\sinh\Omega(L-z)}{\Omega\cosh\Omega L + i(\Delta k)\sinh\Omega L}A(0) \tag{5.11}$$

$$B(z) = e^{-i\Delta kz}\frac{-i\kappa_T\sinh\Omega(L-z)}{\Omega\cosh\Omega L + i(\Delta k)\sinh\Omega L}A(0) \tag{5.12}$$

where $\Omega = \sqrt{\kappa_T^2 - (\Delta k)^2}$. $A(0)$ is the input mode amplitude at $z = 0$.

The parameter Δk is a phase factor and is defined as

$$\Delta k = \frac{\omega}{2c}(n_a + n_b) - \frac{\pi}{d} \tag{5.13}$$

The coupling constant for the same modes (since the waveguides are considered to be identical) of propagation is defined in ref [7] as

$$\kappa_T = \left(\frac{2\pi}{\lambda}\right)^2 \frac{2n_A^2}{\beta w}\left(\frac{(1 - n_m^2/n_A^2)q_m e^{-q_m l_r}}{1 + q_m^2/h_A^2}\right) \tag{5.14}$$

where the parameters h_A and q_m are defined as

$$h_A = \sqrt{\left(\frac{\omega n_A}{c}\right)^2 - \beta^2} \tag{5.15}$$

$$q_m = \sqrt{\beta^2 - \left(\frac{\omega n_s}{c}\right)^2} \tag{5.16}$$

They are the transverse wave vectors for EM waves propagating in the waveguides and NHA structure, respectively. In the above equations, w denotes the width (or diameter) of each waveguide and l_r is the thickness of the NHA structure.

The reflection coefficient of the coupler is given by

$$R = \frac{|B(0)|^2}{|A(0)|^2} \tag{5.17}$$

Putting $z = 0$ in eqns (5.11) and (5.12), we get

$$R = \frac{\kappa_T^2 \sinh^2 \Omega L}{\Omega^2 \cosh^2 \Omega L + (\Delta k)^2 \sinh^2 \Omega L} \tag{5.18}$$

The transmission coefficient is given by

$$T = 1 - R \tag{5.19}$$

Putting eqns (5.18) into eqn (5.19), it becomes

$$T = \frac{\Omega^2 \cosh^2 \Omega L + \left|(\Delta k)^2 - \kappa_T^2\right| \sinh^2 \Omega L}{\Omega^2 \cosh^2 \Omega L + (\Delta k)^2 \sinh^2 \Omega L} \tag{5.20}$$

Let us associate a wavelength with the periodicity of the NHA structure, $\lambda_B = 2a_p$. This is commonly called the Bragg wavelength. This wavelength λ_B has an associated frequency

$$\omega_B = \frac{2\pi c}{n_A \lambda_B} \tag{5.21}$$

where c is the speed of light. Let us call this frequency the Bragg frequency. We can define a detuning parameter from the phase factor, $\delta = \Delta k L$. The detuning parameter can be expressed in terms of the Bragg frequency as

$$\delta = \Delta k L = \frac{(\omega - \omega_B)}{\omega_c} \tag{5.22}$$

where ω_c is defined as

$$\omega_c = \frac{c}{n_A L} \tag{5.23}$$

Note that the detuning parameter, unitless quantity, a nothing more than a quantity which measures the frequency of the EM wave with respect to ω_B , which in turn is obtained from the periodicity of the NHA structure.

5.3 Results and Discussion

In this section, we have performed numerical simulations for the reflection and transmission coefficients of the coupler. Waveguides A and B are made from silica which gives $n_A = n_B = 1.45$. The periodicity of the metallic lattice structure is taken to be $a_p = 200nm$. The metallic lattice made from silver rods. The plasmon frequency for silver is given such that $\hbar\omega_p = 3.93eV$. For simplicity, we have put $\gamma_m = 0$.

Using the above parameters, the values of frequencies ω_B and ω_c are found to give $\hbar\omega_B = 2.85eV$ and $\hbar\omega_c = 0.055eV$ respectively.

We have used a value of the coupling constant κ_T such that $\kappa_T L = 2$. A similar value of the coupling constant has been used in the literature [6].

The reflection and transmission coefficients have been calculated in Figs. 5.2 and 5.3 as a function of the detuning parameter, δ, respectively. Here, the solid and dotted curves correspond to the reflection and transmission coefficient for $L = 2000nm$ and $L = 3000nm$, respectively. Note that near zero detuning, the EM wave is totally reflected through waveguide B.

Note also that as the width of the waveguide changes the reflection coefficient changes. The width of the wave guide can be modified by applying an external pressure and stress. This property can be used for the sensing mechanism.In Fig. 5.4 and Fig. 5.5, we investigate the role of the periodicity of the metallic structure. The reflection and transmission coefficients have been calculated in Figs. 5.4 and 5.5 as a function of the detuning parameter, δ, respectively.The solid curve corresponds to $a_p = 150nm$, whereas the dotted curve corresponds to $a_p = 180nm$. Note that the width of the reflected energy

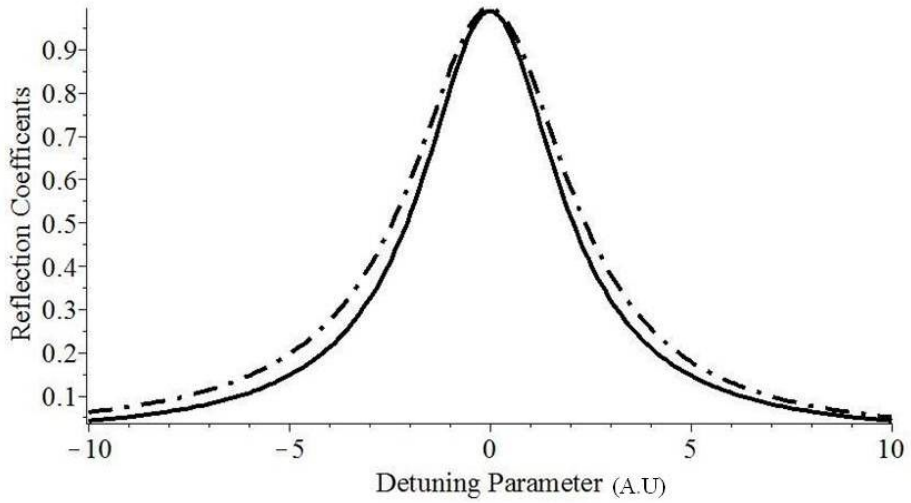

Figure 5.2: Plot of the reflection coefficient as a function of the detuning parameter. The solid curve corresponds to $L = 2000nm$, whereas the dotted curve corresponds to $L = 3000nm$.

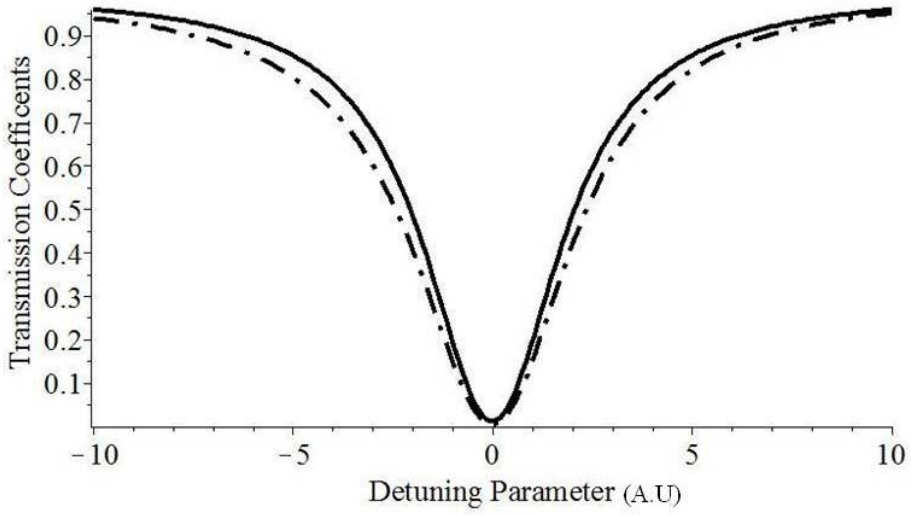

Figure 5.3: Plot of the transmission coefficient as a function of the detuning parameter. The solid curve corresponds to $L = 2000nm$, whereas the dotted curve corresponds to $L = 3000nm$.

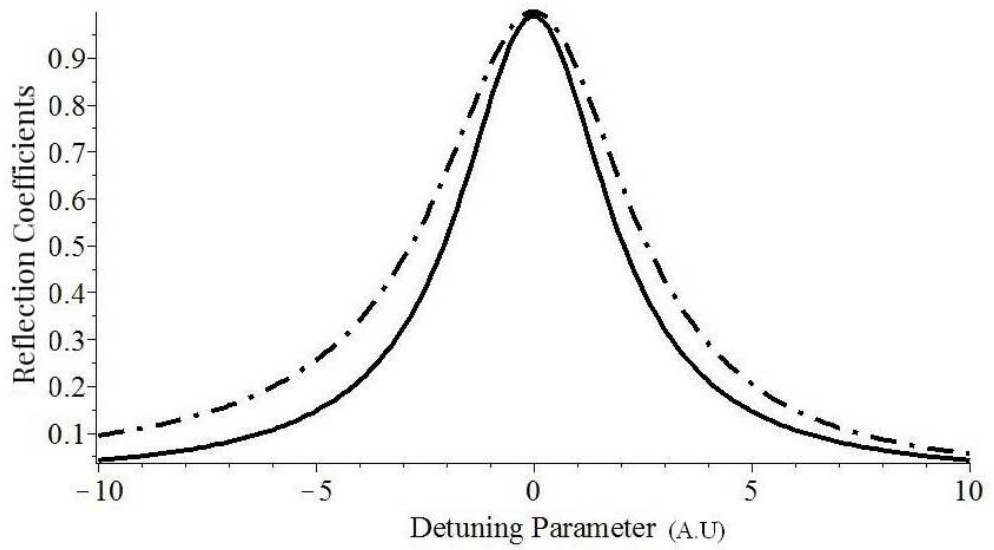

Figure 5.4: Plot of the reflection coefficient as a function of the detuning parameter. The solid curve corresponds to $a_p = 150nm$, whereas the dotted curve corresponds to $a_p = 180nm$.

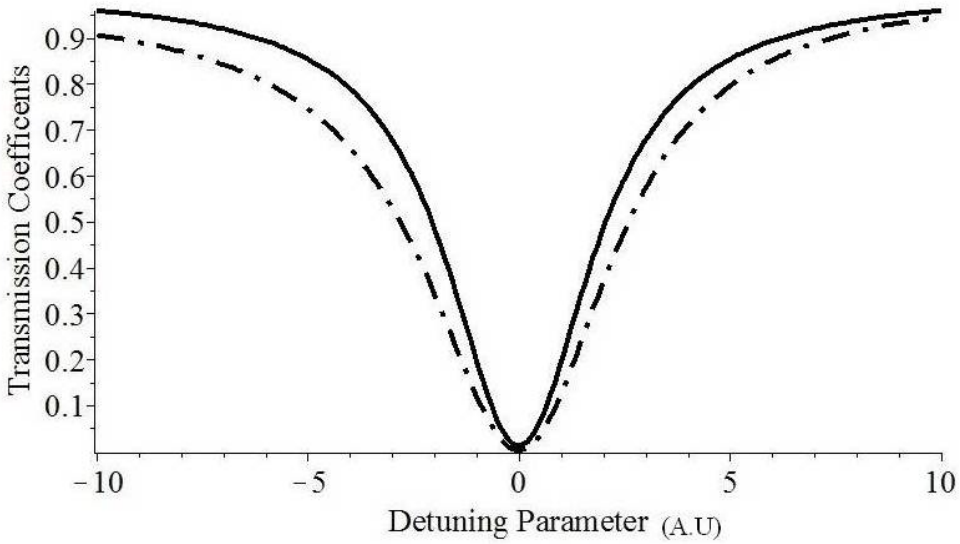

Figure 5.5: Plot of the transmission coefficient as a function of the detuning parameter. The solid curve corresponds to $a_p = 150nm$, whereas the dotted curve corresponds to $a_p = 180nm$.

band has decreased due to the increase in periodicity. It is also worth pointing out that the left band edge has moved to the right. In other words, when the periodicity is changed, some of the reflected light is now transmitted. This means that by changing the periodicity, one can switch the system on and off.

Finally, we note that the inclusion of the loss factor will decrease the heights of the reflection and transmission peaks; the other findings of this paper will not be affected.

5.4 Conclusion

The transmission and reflection properties of a double nanophotonic waveguide have been studied. The two waveguides are coupled by a periodic structure made of alternating layers of a metal and a dielectric material. We consider an EM wave that is propagating in waveguide A, travelling to the left, while in waveguide B the EM wave travels to the right. These two waves couple with each other via the periodic metallic perturbation. Using the transfer matrix method, expressions for the reflection and transmission coefficients have been obtained. Numerical simulations for these coefficients have been carried out. It was found that for certain energies, the EM wave is totally reflected by the coupler and for the certain energies the light is completely transmitted. Thus this system can act as a light filter and light selector. We have shown that by changing the periodicity of the perturbation, the transmitted energy can be reflected. In other words, the system can be used as an optical switch.

Bibliography

[1] Mahi R. Singh, Electronic, photonic, polaritonic and plasmonic materials (Wiley Custom, Toronto, 2014).

[2] G. Brambilla, F. Koizumi, X. Feng and D.J. Richardson, Electronics Letters Vol. 41, No. 7 (31 March, 2005); B. G. Lee et al., IEEE Photonic Tech. Lett. 20, 398 (2008); D. Lauvernier, S. Garidel, M. Zegaoui, J. P. Vilcot and D. Decoster, Electronics Letters Vol. 42, No. 4 (16th February 2006).

[3] D. Decoster et al., Adv. Mat. Res. 31, 230 (2008); M.A. Schmidt et al., Phys. Rev. B 77, 033417 (2008).

[4] M. R. Singh, Appl. Phys. B 93, 91 (2008).

[5] M. R. Singh, J. Phys. B.42, 065503 (2009).

[6] K. Okamoto, Fundamentals of optical waveguides , Academic Press, New York, (2000).

[7] A. Ariv and P. Yeh, Photonics, Oxford University Press, Oxford, (2007).

[8] M. R. Singh, M. Najiminaini, S. Balakrishnan and J. J. L. Carson, J. Appl. Phys. 117 ,

184302 (2015).

Chapter 6

Concluding Remarks

In this thesis, we have studied the light-matter interactions in metallic nano-hole array structure. Numerical calculations were performed on nano-hole array in thin gold film fabricated on Pyrex substrate. The effective dielectric constant of the metallic nano-hole structure calculated using transmission line (TL) theory was used to calculate the dispersion relation. The surface plasmon polariton (SPP) modes present in the nano-hole array structure were found using the dispersion relation and polarizability of the nano-hole array structure. The SPP energies were found to be quantized and it was also found that the systems can have several SPP modes depending on the radius and periodicity of the structure. Using the SPP modes, the scattering cross section of light with normal incident in the nano-hole array structure was calculated for three different samples having unique nano-hole radii and periodicity. There was fairly a good agreement between the theory and experimental results. It is proposed that the theory could be used to optimize nano sensors for medical and engineering applications.

The angle dependence transmission coefficient of the nano-hole array structure was investigated. An expression for angle dependence SPPs was derived using transfer matrix method and Bloch's theorem. The transmission coefficient was calculated using quantum density matrix method. Our calculations predicted that as the angle of incidence increases, the number of peaks increases. It was also found that the transmission peaks either red shifts or blue shifts due to SPP modes and the heights of the peaks are dependent upon the angle of incidence of the light. A good agreement was observed between theoretcial and experimental results.

The transmission and reflecetion coefficient of metallic nano-hole array coupler was studied. The optical sensing mechanism of photonic couplers fabricated from the periodically arranged metallic nano-rods was developed. The metallic nano-hole array structure is embedded between two dielectric material waveguides. Using the transfer matrix method and coupled mode theory, expressions for the reflection and transmission coefficients of electromagnetic wave propagating in waveguides have been obtained. It was found that for certain energies, the electromagnetic wave is totally reflected from the coupler. Similarly, for a certain energy range the light is totally transmitted. It has also been found that by changing the periodicity of the metallic nano-hole array, the transmitted energy can be reflected. The periodicity of the nano-hole array structure can be modified by applying an external stress or pressure. In other words, the system can be used as stress and pressure sensors. The present findings can be used to make new types photonic sensors.

There are many number of possibilities by which the nano-hole array structures can be fabricated. For example, NHA structure can be fabricated by changing the shapes of the

nano-holes, periodicity along the y and z directions, surrounding dielectric material. Many researchers have studied the optical properties of nano-hole structure with a cavity beneath the metallic film. As an immediate step of the present work, the scattering cross section theory and quantum density matrix method could be extended to study the transmission coefficient of light through NHA with a cavity beneath it. The theories can also be extended to study the effect of hole shapes and symmetry of periodicity on transmission. The theory can also be applied to study the effect of pressure waves on the transmission of light through the nano-hole structure.

Chapter 7

Appendices

7.1 Appendix A

7.1.1 Derivation for scattering cross section

In this section the derivation for scattering cross section of light by the metallic NHA on pyrex substrate is explained.

The Hamiltonian of the SPPs in second quantized notation is written as

$$H_{spp} = \sum_{n} \varepsilon_n^{sp} b_n^{+} b_n \tag{7.1}$$

where b_n^{+} and b_n are the creation and annihilation operators of the SPPs, respectively. An eigen ket of H_{spp} is denoted as $|n\rangle$ and the ground state of the SPPs is denoted as $|0\rangle$.

An applied EM field $\mathbf{E}$ induces a dipole moment $\mathbf{d}$ in the nano-hole structure due the absorption and emission of the SPPs. These induced dipoles interact with the applied EM field. The interaction Hamiltonian between photons and the SPPs is written in the

dipole approximation as [1],[2]

$$V_{in} = -\mathbf{d}.\mathbf{E} \tag{7.2}$$

where E_p is the applied EM field which is expressed as

$$\mathbf{E} = \frac{1}{2}\mathbf{E}_0 \left(e^{-i\omega t} + e^{i\omega t}\right) \tag{7.3}$$

In eqn. (7.2), $\mathbf{d}$ is the dipole operator. The dipole operator is expressed in the second quantized form as [1],[2]

$$\mathbf{d} = \sum_n d_n \left(b_n^+ \ + b_n\right) \tag{7.4}$$

where $d_n = \langle n| V_{int} |n\rangle$ is the matrix element of the dipole moment operator. Putting eqns. (7.3) and (7.4) into eqn. (7.2) and using the rotating wave approximation [1],[2] we get the following expression for the interaction Hamiltonian as

$$V_{int} = -\sum_n \frac{1}{2}\mathbf{d}_n.\mathbf{E}_0 \left(b_n^+ e^{-i\omega t} + b_n e^{i\omega t}\right) \tag{7.5}$$

The total Hamiltonian is obtained by adding eqns. (7.1) and (7.5) as

$$H_T = H_{spp} + V_{int} \tag{7.6}$$

$$H_T = \sum_n \varepsilon_n^{sp} b_n^+ \ b_n - \sum_n \frac{1}{2}\mathbf{d}_n.\mathbf{E}_0 \left(b_n^+ e^{-i\omega t} + b_n e^{i\omega t}\right) \tag{7.7}$$

With the help of the total Hamiltonian (i.e. eqn. (7.7)) the scattering cross section is calculated using the quantum mechanical scattering theory and the perturbation theory (i.e. Green's function method) given in reference [1],[2] and it is found as

$$\frac{d\sigma}{d\Omega} d\Omega = \frac{\sum_n w_{in}\rho(\varepsilon)d\Omega}{\frac{1}{2}\epsilon_0 E_0^2} \tag{7.8}$$

where the function $\rho(\varepsilon)$ is called density of states of scattered photons and $\rho(\varepsilon_p)d\Omega$ is the number of photons scattered into the detector with angle $d\Omega$. Here w_{in} is the transition

probability of the system going from the initial state $|i\rangle$ to the final state $|n\rangle$. Using the Green's function method the expression for w_{in} is found as

$$w_{in} = \left(\frac{2\pi}{\hbar}\right) |\langle i| V_{int} |n\rangle|^2 \left(\frac{\Gamma_n}{\left(\varepsilon - \varepsilon_n^{sp}\right)^2 + \Gamma_n^2}\right) \tag{7.9}$$

where the $|i\rangle$ initial state is nothing but the SPP ground state i.e. $|i\rangle = |0\rangle$. Here Γ_n is the linewidth (i.e. decay rate) of the nth SPP eigen ket $|n\rangle$. Putting the expression of V_{int} from eqn. (7.5) into eqn. (7.8) we get

$$w_{in} = \left(\frac{2\pi}{\hbar}\right) \left(\frac{1}{2}\mathbf{d}_n.\mathbf{E}_0\right)^2 \left(\frac{\Gamma_n}{\left(\varepsilon - \varepsilon_n^{sp}\right)^2 + \Gamma_n^2}\right) \tag{7.10}$$

The scattering cross section due to the SPPs can be calculated by putting w_{in} from eqn. (7.9) into eqn. (7.7) and we get

$$\left|\frac{d\sigma}{d\Omega}\right|_{spp} = \sum_n \frac{4\pi \mathbf{d}_n^2 \rho_{spp}\left(\varepsilon_n^{sp}\right)}{\epsilon_0 \hbar} \left(\frac{\Gamma_n}{\left(\varepsilon - \varepsilon_n^{sp}\right)^2 + \Gamma_n^2}\right) \tag{7.11}$$

The density of states $\rho\left(\varepsilon_n^{sp}\right)$ for the SPP mode appearing in the above expression are calculated as

$$\rho_{spp}\left(\varepsilon\right) = \frac{2}{(2\pi)} \frac{dk_z}{d\varepsilon} \tag{7.12}$$

We used eqn. (3.8) to calculate the above expresion of the density of state. Eqn. (7.11) reduces to

$$\rho_{spp}\left(\varepsilon\right) = \frac{2G_n^{'}\left(\varepsilon\right)}{(2\pi)} \tag{7.13}$$

where $G_n^{'}\left(\varepsilon_n^{sp}\right)$ is the energy derivative of $G_n\left(\varepsilon\right)$ at $\varepsilon = \varepsilon_n^{sp}$. Putting the expression of the DOS from eqn. (12) into eqn.(10) we get the final expression of the scattering cross section as

$$\left|\frac{d\sigma}{d\Omega}\right|_{spp} = \sum_n \frac{4d_n^2 G_n'\left(\varepsilon_n^{sp}\right)}{\epsilon_0 \hbar} \left(\frac{\Gamma_n}{\left(\varepsilon_p - \varepsilon_n^{sp}\right)^2 + \Gamma_n^2}\right) \tag{7.14}$$

Similar method gives the expression for scattering cross section of light with bulk plasmon.

7.2 Appendix B

7.2.1 Derivation for matrix elements ρ_{ij}

In this section the derivation of equation of motion for density matrix elements is explained.

The Hamiltonian of SPP modes in the second quantized form is written as [3]

$$H_0 = \varepsilon_0\sigma_{00} + \varepsilon_1\sigma_{11} + \varepsilon_2\sigma_{22} + \varepsilon_3\sigma_{33} + \varepsilon_4\sigma_{44} + \varepsilon_5\sigma_{55} \tag{7.15}$$

where $\sigma_{nn} = |n\rangle\langle n|$ is called the preservation operator.

When an external EM field E_p is applied, dipole moments are induced. The interaction Hamiltonian between photons and induced dipole moments in rotating wave approximation is written as

$$H_F = -\left[\hbar\sum_{n=1}^{5}\Omega_{0n}\sigma_{0n}^{+}e^{-i\frac{(\varepsilon_{n0}-\varepsilon_p)t}{\hbar}}\right] + h.c. \tag{7.16}$$

where $\sigma_{0n}^{+} = |n\rangle\langle 0|$ is the SPP creation operator and $\varepsilon_{n0} = (\varepsilon_n - \varepsilon_0)$. Here $h.c$ stands for the Hermitian conjugate. Parameter Ω_{0n} is called the Rabi frequency associated with the transition between $|0\rangle$ and $|n\rangle$.

The total Hamiltonian of the system is given by

$$H = H_0 + H_F \tag{7.17}$$

$$\begin{aligned} H &= \varepsilon_0\sigma_{00} + \varepsilon_1\sigma_{11} + \varepsilon_2\sigma_{22} + \varepsilon_3\sigma_{33} + \varepsilon_4\sigma_{44} + \varepsilon_5\sigma_{55} \\ &\quad - \left[\hbar\sum_{n=1}^{5}\Omega_{0n}\sigma_{0n}^{+}e^{-i\frac{(\varepsilon_{n0}-\varepsilon_p)t}{\hbar}}\right] + h.c. \end{aligned} \tag{7.18}$$

Considering the interaction representation

$$H_F = e^{-i\frac{H_o t}{\hbar}} H_F e^{+i\frac{H_o t}{\hbar}} \tag{7.19}$$

It follows that

$$H_F = -\hbar \begin{bmatrix} \left(\Omega_{01}\sigma_{10}e^{-i\omega t - i\omega_1 t + i\omega_0 t} + \Omega_{01}^*\sigma_{01}e^{+i\omega t + i\omega_1 t - i\omega_0 t}\right) + \\ \left(\Omega_{02}\sigma_{20}e^{-i\omega t - i\omega_2 t + i\omega_0 t} + \Omega_{02}^*\sigma_{02}e^{+i\omega t + i\omega_2 t - i\omega_0 t}\right) + \\ \left(\Omega_{03}\sigma_{30}e^{-i\omega t - i\omega_3 t + i\omega_0 t} + \Omega_{03}^*\sigma_{03}e^{+i\omega t + i\omega_3 t - i\omega_0 t}\right) + \\ \left(\Omega_{04}\sigma_{40}e^{-i\omega t - i\omega_4 t + i\omega_0 t} + \Omega_{04}^*\sigma_{04}e^{+i\omega t + i\omega_4 t - i\omega_0 t}\right) + \\ \left(\Omega_{05}\sigma_{50}e^{-i\omega t - i\omega_5 t + i\omega_0 t} + \Omega_{05}^*\sigma_{05}e^{+i\omega t + i\omega_5 t - i\omega_0 t}\right) \end{bmatrix} \tag{7.20}$$

We can simplify the above hamiltonians to

$$H_F = -\hbar \begin{bmatrix} \left(\Omega_{01}\sigma_{10}e^{-i\Delta_{10} t} + \Omega_{01}^*\sigma_{01}e^{+i\Delta_{10} t}\right) + \\ \left(\Omega_{02}\sigma_{20}e^{-i\Delta_{20} t} + \Omega_{02}^*\sigma_{02}e^{+i\Delta_{20} t}\right) + \\ \left(\Omega_{03}\sigma_{30}e^{-i\Delta_{30} t} + \Omega_{03}^*\sigma_{03}e^{+i\Delta_{30} t}\right) + \\ \left(\Omega_{04}\sigma_{40}e^{-i\Delta_{40} t} + \Omega_{04}^*\sigma_{04}e^{+i\Delta_{40} t}\right) + \\ \left(\Omega_{05}\sigma_{50}e^{-i\Delta_{50} t} + \Omega_{05}^*\sigma_{05}e^{+i\Delta_{50} t}\right) \end{bmatrix} \tag{7.21}$$

where

$$\Delta_{10} = \omega - (\omega_1 - \omega_0) \tag{7.22}$$

$$\Delta_{20} = \omega - (\omega_2 - \omega_0) \tag{7.23}$$

$$\Delta_{30} = \omega - (\omega_3 - \omega_0) \tag{7.24}$$

$$\Delta_{40} = \omega - (\omega_4 - \omega_0) \tag{7.25}$$

$$\Delta_{50} = \omega - (\omega_5 - \omega_0)$$

where the density matrix element is

$$\frac{d\tilde{\rho}}{dt} = -\frac{i}{\hbar}\left[H_F, \tilde{\rho}\right] \tag{7.26}$$

$$\tilde{\rho}_{mn} = \langle m|\tilde{\rho}|n\rangle \tag{7.27}$$

We are only considering the interaction terms because of the interaction representation. With this information we are able to calculate the density matrix operators for each state. Let us consider ρ_{55}

$$\left\langle 5 \left| \frac{d\tilde{\rho}}{dt} \right| 5 \right\rangle = \left\langle 5 \left| -\frac{i}{\hbar} \left[H_F, \tilde{\rho} \right] \right| 5 \right\rangle \tag{7.28}$$

$$i\hbar \frac{d\tilde{\rho_{55}}}{dt} = \left\langle 5 \left| \left[H_F, \tilde{\rho} \right] \right| 5 \right\rangle \tag{7.29}$$

Let us calculate each section seperately

$$A = \left\langle 5 \left| \left[H_F, \tilde{\rho} \right] \right| 5 \right\rangle \tag{7.30}$$

Now we recalling the commutation of operators

$$[X, Y] = XY - YX \tag{7.31}$$

With this we can solve the following term

$$A = \left\langle 5 \left| \left[H_F, \tilde{\rho} \right] \right| 5 \right\rangle \tag{7.32}$$

$$A = \left\langle 5 \left| H_F \tilde{\rho} - \tilde{\rho} H_F \right| 5 \right\rangle \tag{7.33}$$

We must multiply by one $\Sigma_i |i\rangle\langle i| = 1$

$$
\begin{aligned}
A &= \left\langle 5 \left| H_F \left(\Sigma_i |i\rangle \langle i| \right) \tilde{\rho} - \tilde{\rho} \left(\Sigma_i |i\rangle \langle i| \right) H_F \right| 5 \right\rangle && (7.34) \\
&= \left\langle 5 \left| \begin{array}{c} H_F \left(|0\rangle\langle 0| + |1\rangle\langle 1| + |2\rangle\langle 2| + |3\rangle\langle 3| + |4\rangle\langle 4| + |5\rangle\langle 5| \right) \tilde{\rho} \\ -\tilde{\rho} \left(|0\rangle\langle 0| + |1\rangle\langle 1| + |2\rangle\langle 2| + |3\rangle\langle 3| + |4\rangle\langle 4| + |5\rangle\langle 5| \right) \tilde{\rho} H_F \end{array} \right| 5 \right\rangle && (7.35) \\
&= \left\langle 5 \left| H_F |0\rangle\langle 0| \tilde{\rho} \right| 5 \right\rangle + \left\langle 5 \left| H_F |1\rangle\langle 1| \tilde{\rho} \right| 5 \right\rangle + \left\langle 5 \left| H_F |2\rangle\langle 2| \tilde{\rho} \right| 5 \right\rangle \\
&\quad + \left\langle 5 \left| H_F |3\rangle\langle 3| \tilde{\rho} \right| 5 \right\rangle + \left\langle 5 \left| H_F |4\rangle\langle 4| \tilde{\rho} \right| 5 \right\rangle + \left\langle 5 \left| H_F |5\rangle\langle 5| \tilde{\rho} \right| 5 \right\rangle \\
&\quad - \left\langle 5 \left| \tilde{\rho} |0\rangle\langle 0| H_F \right| 5 \right\rangle - \left\langle 5 \left| \tilde{\rho} |1\rangle\langle 1| H_F \right| 5 \right\rangle - \left\langle 5 \left| \tilde{\rho} |2\rangle\langle 2| H_F \right| 5 \right\rangle \\
&\quad - \left\langle 5 \left| \tilde{\rho} |3\rangle\langle 3| H_F \right| 5 \right\rangle - \left\langle 5 \left| \tilde{\rho} |4\rangle\langle 4| H_F \right| 5 \right\rangle - \left\langle 5 \left| \tilde{\rho} |5\rangle\langle 5| H_F \right| 5 \right\rangle && (7.36) \\
&= \langle 5|H_F|0\rangle \tilde{\rho}_{05} + \langle 5|H_F|1\rangle \tilde{\rho}_{15} + \langle 5|H_F|2\rangle \tilde{\rho}_{25} + \\
&\quad \langle 5|H_F|3\rangle \tilde{\rho}_{35} + \langle 5|H_F|4\rangle \tilde{\rho}_{45} + \langle 5|H_F|5\rangle \tilde{\rho}_{55} \\
&\quad - \tilde{\rho}_{50} \langle 0|H_F|5\rangle - \tilde{\rho}_{51} \langle 1|H_F|5\rangle - \tilde{\rho}_{52} \langle 2|H_F|5\rangle \\
&\quad - \tilde{\rho}_{53} \langle 3|H_F|5\rangle - \tilde{\rho}_{54} \langle 4|H_F|5\rangle - \tilde{\rho}_{55} \langle 5|H_F|5\rangle && (7.37)
\end{aligned}
$$

To solve the above set of equations we need to remember H_F

$$
H_F = -\hbar \begin{bmatrix} \left(\Omega_{01}\sigma_{10}e^{-i\Delta_{10}t} + \Omega_{01}^*\sigma_{01}e^{+i\Delta_{10}t} \right) + \\ \left(\Omega_{02}\sigma_{20}e^{-i\Delta_{20}t} + \Omega_{02}^*\sigma_{02}e^{+i\Delta_{20}t} \right) + \\ \left(\Omega_{03}\sigma_{30}e^{-i\Delta_{30}t} + \Omega_{03}^*\sigma_{03}e^{+i\Delta_{30}t} \right) + \\ \left(\Omega_{04}\sigma_{40}e^{-i\Delta_{40}t} + \Omega_{04}^*\sigma_{04}e^{+i\Delta_{40}t} \right) + \\ \left(\Omega_{05}\sigma_{50}e^{-i\Delta_{50}t} + \Omega_{05}^*\sigma_{05}e^{+i\Delta_{50}t} \right) \end{bmatrix} \qquad (7.38)
$$

where $\sigma_{mn} = |m\rangle\langle n|$

$$\begin{aligned}
\langle 5|H_F|0\rangle &= \left\langle 5 \left| -\hbar \begin{bmatrix} \left(|1\rangle\langle 0|\Omega_{01}e^{-i\Delta_{10}t} + |0\rangle\langle 1|\Omega_{01}^* e^{+i\Delta_{10}t}\right) + \\ \left(|2\rangle\langle 0|\Omega_{02}e^{-i\Delta_{20}t} + |0\rangle\langle 2|\Omega_{02}^* e^{+i\Delta_{20}t}\right) + \\ \left(|3\rangle\langle 0|\Omega_{03}e^{-i\Delta_{30}t} + |0\rangle\langle 3|\Omega_{03}^* e^{+i\Delta_{30}t}\right) \\ + \left(|4\rangle\langle 0|\Omega_{04}e^{-i\Delta_{40}t} + |0\rangle\langle 4|\Omega_{04}^* e^{+i\Delta_{40}t}\right) + \\ \left(|5\rangle\langle 0|\Omega_{05}e^{-i\Delta_{50}t} + |0\rangle\langle 5|\Omega_{05}^* e^{+i\Delta_{50}t}\right) \end{bmatrix} \right| 0 \right\rangle \qquad (7.39) \\
&= 0+0+0+0+0+0+0+0+\Omega_{05}e^{-i\Delta_{50}t}+0 \\
\langle 5|H_F|0\rangle &= -\hbar\Omega_{05}e^{-i\Delta_{50}t} \\
\langle 5|H_F|1\rangle &= \langle 5|H_F|2\rangle = \langle 5|H_F|3\rangle = \langle 5|H_F|4\rangle = \langle 5|H_F|5\rangle = 0 \\
\langle 0|H_F|5\rangle &= -\hbar\Omega_{05}^* e^{+i\Delta_{50}t} \\
\langle 1|H_F|5\rangle &= \langle 2|H_F|5\rangle = \langle 3|H_F|5\rangle = \langle 4|H_F|5\rangle = \langle 5|H_F|5\rangle = 0
\end{aligned}$$

Thus

$$A = -\Omega_{05}e^{-i\Delta_{50}t}\tilde{\rho}_{05} + \tilde{\rho}_{50}\Omega_{05}^* e^{+i\Delta_{50}t} \qquad (7.40)$$

Finally, we can collect all the terms. We get the following equation of motion

$$\begin{aligned}
i\hbar\frac{d\tilde{\rho}_{55}}{dt} &= \left\langle 5 \left| \left[H_F, \tilde{\rho}\right] \right| 5 \right\rangle \qquad (7.41) \\
&= A \\
&= -\hbar\Omega_{05}e^{-i\Delta_{50}t}\tilde{\rho}_{05} + \hbar\tilde{\rho}_{50}\Omega_{05}^* e^{+i\Delta_{50}t} \qquad (7.42)
\end{aligned}$$

We can further simplify the equations by substituting the following

$$\tilde{\rho_{55}} = \rho_{55} \tag{7.43}$$

$$\tilde{\rho_{05}} = \rho_{05} e^{+i\Delta_{05}t} \tag{7.44}$$

$$\tilde{\rho_{50}} = \rho_{50} e^{-i\Delta_{50}t} \tag{7.45}$$

The new equations take the form as

$$\frac{d\rho_{55}}{dt} = +i\left(\Omega_{05}\right)\rho_{05} - i\left(\Omega_{05}\right)^{*}\rho_{50} \tag{7.46}$$

Including the radiative linewidth of the state we get the following

$$\frac{d\rho_{55}}{dt} = -2\Gamma_5\rho_{55} + i\left(\Omega_{05}\right)\rho_{05} - i\left(\Omega_{05}\right)^{*}\rho_{50} \tag{7.47}$$

Using the same method we would get the equation of motion for other density matrix elements ρ_{jj}

Now, let us consider ρ_{50}

$$\left\langle 5 \left| \frac{d\tilde{\rho}}{dt} \right| 0 \right\rangle = \left\langle 5 \left| -\frac{i}{\hbar}\left[H_F, \tilde{\rho}\right] \right| 0 \right\rangle \tag{7.48}$$

$$i\hbar\frac{d\tilde{\rho_{50}}}{dt} = \left\langle 5 \left| \left[H_F, \tilde{\rho}\right] \right| 0 \right\rangle \tag{7.49}$$

Let us calculate each section seperately

$$A = \left\langle 5 \left| \left[H_F, \tilde{\rho}\right] \right| 0 \right\rangle \tag{7.50}$$

Now we must remember the commutation of operators

$$[X, Y] = XY - YX \tag{7.51}$$

With this we can solve the following term

$$A = \left\langle 5 \left| \left[H_F, \tilde{\rho} \right] \right| 0 \right\rangle \tag{7.52}$$

$$A = \left\langle 5 \left| H_F \tilde{\rho} - \tilde{\rho} H_F \right| 0 \right\rangle \tag{7.53}$$

We must multiply by one $\Sigma_i |i\rangle\langle i| = 1$

$$A = \left\langle 5 \left| H_F \left(\Sigma_i |i\rangle \langle i| \right) \tilde{\rho} - \tilde{\rho} \left(\Sigma_i |i\rangle \langle i| \right) H_F \right| 0 \right\rangle \tag{7.54}$$

$$= \left\langle 5 \left| \begin{array}{c} H_F \left(|0\rangle\langle 0| + |1\rangle\langle 1| + |2\rangle\langle 2| + |3\rangle\langle 3| + |4\rangle\langle 4| + |5\rangle\langle 5| \right) \tilde{\rho} \\ -\tilde{\rho} \left(|0\rangle\langle 0| + |1\rangle\langle 1| + |2\rangle\langle 2| + |3\rangle\langle 3| + |4\rangle\langle 4| + |5\rangle\langle 5| \right) H_F \end{array} \right| 0 \right\rangle \tag{7.55}$$

$$\begin{aligned} = & \left\langle 5 \left| H_F |0\rangle\langle 0| \tilde{\rho} \right| 0 \right\rangle + \left\langle 5 \left| H_F |1\rangle\langle 1| \tilde{\rho} \right| 0 \right\rangle + \left\langle 5 \left| H_F |2\rangle\langle 2| \tilde{\rho} \right| 0 \right\rangle \\ & + \left\langle 5 \left| H_F |3\rangle\langle 3| \tilde{\rho} \right| 0 \right\rangle + \left\langle 5 \left| H_F |4\rangle\langle 4| \tilde{\rho} \right| 0 \right\rangle + \left\langle 5 \left| H_F |5\rangle\langle 5| \tilde{\rho} \right| 0 \right\rangle \\ & - \left\langle 5 \left| \tilde{\rho} |0\rangle\langle 0| H_F \right| 0 \right\rangle - \left\langle 5 \left| \tilde{\rho} |1\rangle\langle 1| H_F \right| 0 \right\rangle - \left\langle 5 \left| \tilde{\rho} |2\rangle\langle 2| H_F \right| 0 \right\rangle \\ & - \left\langle 5 \left| \tilde{\rho} |3\rangle\langle 3| H_F \right| 0 \right\rangle - \left\langle 5 \left| \tilde{\rho} |4\rangle\langle 4| H_F \right| 0 \right\rangle - \left\langle 5 \left| \tilde{\rho} |5\rangle\langle 5| H_F \right| 0 \right\rangle \end{aligned} \tag{7.56}$$

$$\begin{aligned} = & \langle 5| H_F |0\rangle \rho_{00} + \langle 5| H_F |1\rangle \rho_{10} + \langle 5| H_F |2\rangle \rho_{20} + \langle 5| H_F |3\rangle \rho_{30} + \\ & \langle 5| H_F |4\rangle \rho_{40} + \langle 5| H_F |5\rangle \rho_{50} \\ & - \langle 0| H_F |0\rangle \rho_{50} - \langle 1| H_F |0\rangle \rho_{51} - \langle 2| H_F |0\rangle \rho_{52} - \langle 3| H_F |0\rangle \rho_{53} - \\ & \langle 4| H_F |1\rangle \rho_{54} - \langle 5| H_F |1\rangle \rho_{55} \end{aligned} \tag{7.57}$$

To solve the above set of equations we need to remember H_F

$$H_F = -\hbar \begin{bmatrix} \left(\Omega_{01} \sigma_{10} e^{-i\Delta_{10} t} + \Omega_{01}^* \sigma_{01} e^{+i\Delta_{10} t} \right) + \\ \left(\Omega_{02} \sigma_{20} e^{-i\Delta_{20} t} + \Omega_{02}^* \sigma_{02} e^{+i\Delta_{20} t} \right) + \\ \left(\Omega_{03} \sigma_{30} e^{-i\Delta_{30} t} + \Omega_{03}^* \sigma_{03} e^{+i\Delta_{30} t} \right) + \\ \left(\Omega_{04} \sigma_{40} e^{-i\Delta_{40} t} + \Omega_{04}^* \sigma_{04} e^{+i\Delta_{40} t} \right) + \\ \left(\Omega_{05} \sigma_{50} e^{-i\Delta_{50} t} + \Omega_{05}^* \sigma_{05} e^{+i\Delta_{50} t} \right) \end{bmatrix} \tag{7.58}$$

where $\sigma_{mn} = |m\rangle\langle n|$

$$\langle 5\,|H_F|\,0\rangle = \left\langle 5\left|\hbar\left[\begin{array}{c}\left(|1\rangle\langle 0|\Omega_{01}e^{-i\Delta_{10}t}+|0\rangle\langle 1|\Omega_{01}^{*}e^{+i\Delta_{10}t}\right)\\ +\left(|2\rangle\langle 0|\Omega_{02}e^{-i\Delta_{20}t}+|0\rangle\langle 2|\Omega_{02}^{*}e^{+i\Delta_{20}t}\right)\\ +\left(|3\rangle\langle 0|\Omega_{03}e^{-i\Delta_{30}t}+|0\rangle\langle 3|\Omega_{03}^{*}e^{+i\Delta_{30}t}\right)\\ +\left(|4\rangle\langle 0|\Omega_{04}e^{-i\Delta_{40}t}+|0\rangle\langle 4|\Omega_{04}^{*}e^{+i\Delta_{40}t}\right)\\ +\left(|5\rangle\langle 0|\Omega_{05}e^{-i\Delta_{50}t}+|0\rangle\langle 5|\Omega_{05}^{*}e^{+i\Delta_{50}t}\right)\end{array}\right]\right|0\right\rangle \tag{7.59}$$

$$= 0+0+0+0+0+0+0+0+0+\Omega_{05}e^{-i\Delta_{50}t}+0 \tag{7.60}$$

$$\langle 5\,|H_F|\,1\rangle = \langle 5\,|H_F|\,2\rangle = \langle 5\,|H_F|\,3\rangle = \langle 5\,|H_F|\,4\rangle = \langle 5\,|H_F|\,5\rangle = 0$$

$$\langle 1\,|H_F|\,0\rangle = \Omega_{01}e^{-i\Delta_{10}t}, \langle 2\,|H_F|\,0\rangle = \Omega_{02}e^{-i\Delta_{20}t}, \langle 3\,|H_F|\,0\rangle = \Omega_{03}e^{-i\Delta_{30}t},$$

$$\langle 4\,|H_F|\,0\rangle = \Omega_{04}e^{-i\Delta_{40}t}$$

Thus

$$A = \Omega_{05}e^{-i\Delta_{50}t}\left(\tilde{\rho_{55}}-\tilde{\rho_{00}}\right)+\hbar\Omega_{01}e^{-i\Delta_{10}t}\rho_{51}\ +\hbar\Omega_{02}e^{-i\Delta_{20}t}\tilde{\rho_{52}}+\hbar\Omega_{03}e^{-i\Delta_{30}t}\tilde{\rho_{53}}+\hbar\Omega_{04}e^{-i\Delta_{40}t}\tilde{\rho_{54}} \tag{7.61}$$

Finally, we can collect all the terms. We get the following equation of motion.

$$i\hbar\frac{d\tilde{\rho_{50}}}{dt} = \left\langle 5\left|\left[H_F,\tilde{\rho}\right]\right|0\right\rangle \tag{7.62}$$

$$= A \tag{7.63}$$

$$\frac{d\tilde{\rho_{50}}}{dt} = -i\Omega_{05}e^{-i\Delta_{50}t}\left(\tilde{\rho_{55}}-\tilde{\rho_{00}}\right)$$

$$-i(\Omega_{01}e^{-i\Delta_{10}t})\rho_{51}-i(\Omega_{02}e^{-i\Delta_{20}t})\tilde{\rho_{52}}-i(\Omega_{03}e^{-i\Delta_{30}t})\tilde{\rho_{53}}-i(\Omega_{04}e^{-i\Delta_{40}t})\tilde{\rho_{54}}$$

We can further simplify the equations by substituting the following

$$\tilde{\rho_{55}} = \rho_{55} \tag{7.64}$$

$$\tilde{\rho_{50}} = \rho_{50} e^{-i\Delta_{50}t} \tag{7.65}$$

$$\tilde{\rho_{51}} = \rho_{51} e^{-i\Delta_{50}t + i\Delta_{10}t} \tag{7.66}$$

By taking into consideration

$$\frac{d(\rho_{50}e^{-i\Delta_{50}t})}{dt} = \frac{d(\rho_{50})}{dt}e^{-i\Delta_{50}t} + \rho_{50}\frac{d(e^{-i\Delta_{50}t})}{dt} \tag{7.67}$$

$$= \frac{d(\rho_{50})}{dt}e^{-i\Delta_{50}t} - i\Delta_{50}\rho_{50}(e^{-i\Delta_{50}t}) \tag{7.68}$$

Including the radiative linewidth we get the following

$$\frac{d\rho_{50}}{dt} = -\left(\frac{\Gamma_5}{2} + i\Delta_{50}\right)\rho_{50} - i\Omega_{05}\left(\tilde{\rho_{55}} - \tilde{\rho_{00}}\right) - i(\Omega_{01})\rho_{51} - i(\Omega_{02})\tilde{\rho_{52}} - i(\Omega_{03})\tilde{\rho_{53}} - i(\Omega_{04})\tilde{\rho_{54}} \tag{7.69}$$

Using the same method we would get the equation of motion for other density matrix elements.

Bibliography

[1] M. R. Singh, *Advanced Quantum Mechanics* (John Wiley and Sons, Toronto, 2014).

[2] J. J. Sakurai and J. Napolitano, *Modern Quantum Mechanics* (Addison-Wesley, 1994).

[3] M. R. Singh, *Electronic, Photonic, Polaritonic and Plasmonic Materials* (John Wiley and Sons, Toronto, 2014).

Shankar Anandh < . @gmail.com>

Permission to Use Copyrighted Material in a Master's Thesis

AIPRights Permissions < @aip.org> Mon, Aug 17, 2015 at 10:31 AM
To: Shankar Anandh < @gmail.com>

Dear Dr. Balakrishnan:

Thank you for requesting permission to reproduce material from AIP Publishing LLC publications.

Material to be reproduced:

"Metamaterial based theoretical description of light scattering by metallic nano-hole array structures" in Journal of Applied Physics , Volume 117, page 184302 (2015)

For use in the following manner:

Reproduced in your Master's thesis entitled, "Transmission of light in nanohole metamaterials," for submission to the University of Western Ontario. It is understood that the thesis will be available in full-text on the Internet for reference, study and/or copy, and that it will be accessible through the Western Libraries site, as well as through Library and Archives Canada and ProQuest/UMI as single copies for sale on demand.

Permission is granted subject to these conditions:

1. AIP Publishing LLC grants you non-exclusive world rights in all languages and media. This permission extends to all subsequent and future editions of the new work.

2. The following copyright notice must appear with the material (please fill in the information indicated by capital letters):

"Reproduced with permission from [FULL CITATION]. Copyright [PUBLICATION YEAR], AIP Publishing LLC."

When reusing a full article, the copyright notice must be printed on the first page of the reprinted article or book chapter. When reusing figures, photographs, covers, or tables, the notice may appear in the caption, in a footnote, or in the reference list.

In cases where the new publication is licensed under a Creative Commons license, the full copyright notice as stated above must appear with the reproduced material.

3. If the material is published in electronic format, we ask that a link be created pointing back to the abstract of the article on the journal website. This can be accomplished through the use of the article's DOI.

4. This permission does not apply to any materials credited to another source.

Please let us know if you have any questions.

Sincerely,

Susann Brailey

Manager, Rights and Permissions

AIP Publishing LLC

1305 Walt Whitman Road

Suite 300

Melville, NY 11747-4300

Tel. +1 516-576-2268

rights@aip.org

From: Shankar Anandh [mailto: . r @gmail.com]
Sent: Friday, August 14, 2015 12:35 PM
To: AIPRights Permissions
Subject: Permission to Use Copyrighted Material in a Master's Thesis

Shankar Anandh < . @gmail.com>

Permission to Use Copyrighted Material in a Master's Thesis

AIPRights Permissions < i t @aip.org> Mon, Aug 17, 2015 at 10:26 AM
To: Shankar Anandh < . r @gmail.com>

Dear Dr. Balakrishnan:

Thank you for requesting permission to reproduce material from AIP Publishing LLC publications.

Material to be reproduced:

"Simulations of optical sensors fabricated from metallic rods couplers," AIP. Conf. Proc., Volume 1590, page 271 (2014)

For use in the following manner:

Reproduced in your Master's thesis entitled, "Transmission of light in nanohole metamaterials," for submission to the University of Western Ontario. It is understood that the thesis will be available in full-text on the Internet for reference, study and/or copy, and that it will be accessible through the Western Libraries site, as well as through Library and Archives Canada and ProQuest/UMI as single copies for sale on demand.

Permission is granted subject to these conditions:

1. AIP Publishing LLC grants you non-exclusive world rights in all languages and media. This permission extends to all subsequent and future editions of the new work.

2. The following copyright notice must appear with the material (please fill in the information indicated by capital letters):

"Reproduced with permission from [FULL CITATION]. Copyright [PUBLICATION YEAR], AIP Publishing LLC."

When reusing a full article, the copyright notice must be printed on the first page of the reprinted article or book chapter. When reusing figures, photographs, covers, or tables, the notice may appear in the caption, in a footnote, or in the reference list.

In cases where the new publication is licensed under a Creative Commons license, the full copyright notice as stated above must appear with the reproduced material.

3. If the material is published in electronic format, we ask that a link be created pointing back to the abstract of the article on the journal website. This can be accomplished through the use of the article's DOI.

4. This permission does not apply to any materials credited to another source.

Please let us know if you have any questions.

Sincerely,

Susann Brailey

Manager, Rights and Permissions

AIP Publishing LLC

1305 Walt Whitman Road

Suite 300

Melville, NY 11747-4300

Tel. +1 516-576-2268

rights@aip.org

From: Shankar Anandh [mailto: r @gmail.com]
Sent: Friday, August 14, 2015 12:05 PM
To: AIPRights Permissions
Subject: Permission to Use Copyrighted Material in a Master's Thesis

Curriculum Vitae

Name: Shankaranandh Balakrishnan

Post-secondary Education and Degrees:

Sri Sathya Sai Institute of Higher Learning
Brindavan campus, Bangalore, India
2007-2010 B.Sc (Hons.) Physics.

Sri Sathya Sai Institute of Higher Learning
Prashanti nilayam campus, Puttaparthi, India
2010-2012 M.Sc Physics

The University of Western Ontario
London, Ontario, Canada
2013-Present M.Sc Physics

Related Work Experience

Teaching Assistant
The University of Western Ontario
2013-2015

Publications:

1. M. R. Singh, Shankar Balakrishnan, "Simulations of optical sensors fabricated from metallic rods couplers" AIP Conf. Proc. **1590**, 271 (2014).
2. Mahi R. Singh, Mohamadreza Najiminaini, Shankar Balakrishnan, Jeffrey J. L. Carson, "Metamaterial based theoretical description of light scattering in metallic nano-hole array structures", J. Appl. Phys. **117**, 184302 (2015).
3. Shankar Balakrishnan, Mohamadreza Najiminaini, Mahi R. Singh, Jeffrey J. L. Carson, "Transmission coefficient of light in nano-hole array structure" to be submitted to J. Appl. Phys. (2015).